ACS OMEGA

http://pubs.acs.org/journal/acsodf

Review

Doped Ceria Nanomaterials: Preparation, Properties, and Uses

Khadijat Olabisi Abdulwahab, Mohammad Mansoob Khan,* and James Robert Jennings*

Cite This: https://doi.org/10.1021/acsomega.3c01199

Read Online

ACCESS | Metrics & More | Article Recommendations

ABSTRACT: Doping is a powerful strategy for enhancing the performance of ceria (CeO_2) nanomaterials in a range of catalytic, photocatalytic, biomedical, and energy applications. The present review summarizes recent developments in the doping of ceria nanomaterials with metal and non-metal dopants for selected applications. The most important metal dopants are grouped into s, p, d, and f block elements, and the relevant synthetic methods, novel properties, and key applications of metal doped ceria are collated and critically discussed. Non-metal dopants are similarly examined and compared with metal dopants using the same performance criteria. The review reveals that non-metal (N, S, P, F, and Cl) doped ceria has mainly been synthesized by calcination and hydrothermal methods, and it has found applications mostly in photocatalysis or as a cathode material for LiS batteries. In contrast, metal doped ceria nanomaterials have been prepared by a wider range of synthetic routes and evaluated for a larger number of applications, including as catalysts or photocatalysts, as antibacterial agents, and in devices such as fuel cells, gas sensors, and colorimetric detectors. Dual/co-doped ceria containing both metals and non-metals are also reviewed, and it is found that co-doping often leads to improved properties compared with single-element doping. The review concludes with a future outlook that identifies unaddressed issues in the synthesis and applications of doped ceria nanomaterials.

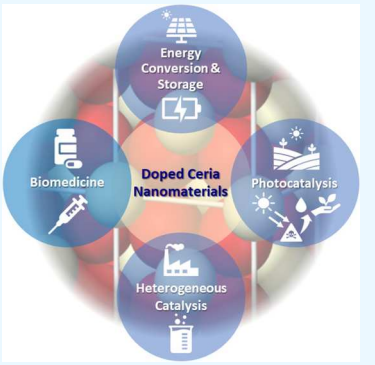

1. INTRODUCTION

Cerium (Ce) is among the most abundant of the rare earth elements. The element has two stable oxidation states, +3 and +4, which arise from its unique electronic configuration of $[Xe]4f^15d^16s^2$. The reaction between Ce and O_2 can lead to the formation of different oxide phases depending on reaction parameters such as temperature and pressure, but the most common oxides are Ce_2O_3 and CeO_2.[1] Cerium(IV) oxide (CeO_2), or ceria, is the most stable of these oxides and has a cubic fluorite structure. In the cubic fluorite structure, eight oxide ions (O^{2-}) surround each Ce^{4+} ion at the cube corners, and four cations coordinate each anion to form a tetrahedron. Pure CeO_2 is a pale-yellow color due to charge transfer between the Ce^{4+} and O^{2-} ions. At high temperatures, ceria is known to undergo a reduction reaction without a change in crystalline phase but with a noticeable color change from yellow to blue or black, depending on the density of oxygen vacancies.[2]

In nanomaterials, surface defects become more pronounced compared with the bulk, because the fraction of surface atoms increases with the decreasing size of the particle. This surface effect leads to the emergence of interesting properties including a high capacity for oxygen release and storage, good catalytic activity, high refractive index, high transparency in the visible region, and strong UV absorption[3,4] These characteristics have been exploited in various applications including catalysis of three-way reactions to mitigate toxic exhaust gases from automobiles, water−gas shift reactions at low temperature, oxygen sensors, oxygen-permeable membranes, fuel cells, supercapacitors,[5] cancer therapy, photocatalytic pollutant degradation, and polishing agents,[6,7] These diverse applications have prompted the synthesis of ceria by numerous routes including hydrothermal synthesis, co-precipitation, microwave-assisted synthesis, and green synthesis.[8,9]

Over the last decade, interest in the preparation of doped ceria nanomaterials has increased. When ceria is doped, extrinsic defects are introduced into its crystal structure, oxygen vacancies are produced, and oxygen migration is improved, all of which lead to enhanced properties.[10] The doping can be achieved by introducing a metal or non-metal dopant.[11−15] The advantages of doping include but are not limited to the fact that the catalytic activity is enhanced. One way this can be achieved is by doping with group 1 or 2 metals of high ionic mobility, which act as shallow electron traps that inhibit the electron−hole recombination process. Furthermore, doping with rare earth metals leads to weaker metal−oxygen bonding, which also favors superior catalytic properties.[16] In addition, oxygen vacancies in doped ceria nanoparticles (NPs)

Received: February 22, 2023
Accepted: June 1, 2023

could be used as probes to sense the radicals produced when they are transferred by a hopping mechanism.[17] Dopant addition can also disrupt chemical bonding on the surface of NPs, thereby creating new active centers that will enhance the selectivity and stability of the resulting doped catalyst.[18]

Several reviews have been written on ceria nanomaterials, doped ceria, and ceria-based composite nanomaterials, in which the fundamental aspects of the redox, acid−base, and catalytic properties of ceria-based materials have been discussed extensively.[1,19] Many authors have also reviewed approaches for improving the catalytic activity of ceria-based composites in photocatalytic CO_2 conversion,[20] NO reduction,[21,22] energy conversion and storage,[23−25] water purification,[26] and gaseous pollutant purification,[6,27] Furthermore, strategies for encapsulation of metal NPs by ceria nanoshells using appropriate synthetic routes have been discussed and their catalytic properties highlighted.[28] The modification and catalytic mechanisms of effective ceria-based photocatalysts for organic pollutant degradation have also been reviewed recently.[16,29]

Although many reviews covering ceria, doped ceria, and ceria-based nanomaterials already exist, these reviews focus on doped ceria for only one or at most a few specific applications. So far, there has not been a systematic review covering all known dopants (metals and non-metals) and applications. Given the above, this review aims to compile and critically discuss all of the different types of dopants, preparation methods, novel properties, and the diverse range of applications of doped ceria. The dopants are grouped and discussed under different headings; metal doped (s block, d block, and f block elements, and dual/co-doped) and non-metal doped ceria, in order to establish a relationship between the chemistry of the dopant and the properties and applications of doped ceria. The review concludes with a discussion of the prospects and challenges associated with achieving optimized performance for doped ceria in its various applications.

2. PROPERTIES OF CERIA

The diverse applications of ceria stem from its varied physical and chemical properties, including redox properties such as the low redox potential of the transition between Ce^{3+} and Ce^{4+} in the cubic fluorite structure, unusual acid−base properties, high oxygen storage capacity (OSC), and interesting optical properties.[19] The density, coordination, and structure of cationic and anionic surface sites, in addition to vacancies and other defects, can be controlled by changing the morphologies of ceria NPs. The particle morphology in turn depends on the synthesis route employed, which can be selected to target specific applications[4,30,31]

2.1. Optical Properties of Ceria. Ceria is an n-type semiconductor with an experimentally observed optical band gap of ∼3.2 eV. However, the assignment of the main optical transition associated with this band gap has proved somewhat controversial,[24] partly due to the varying abilities of common density functional theory methods to reproduce the localization of Ce 4f electrons and subsequent polaron formation.[32] It is currently thought that the observed band gap arises mainly from an O 2p → Ce 4f transition, which is expected to occur between fully occupied O 2p states and empty Ce 4f states.[24,33] The band gap of ∼3.2 eV means that ceria only absorbs ultraviolet (UV) light of wavelengths <390 nm. Another interesting optical property of ceria is its high refractive index, which is in the range 2.2−2.8 at 632 nm. Such a high refractive index makes ceria useful in the manufacturing of glasses, filters, and optoelectronic devices.[34−36]

In order to enhance the performance of ceria in photocatalytic applications, the light absorption range must be expanded to the visible region, which can be achieved by doping, by forming a composite or heterojunction, or by manipulating the synthesis route to generate defects in the structure.[29,37−39] For instance, Khan and co-workers synthesized ceria using the electron beam irradiation method.[40] By subjecting the commercial ceria to two different doses of electrons, the electron beam technique achieved "defect engineering", and the resulting modified ceria particles were compared with pristine ceria. Electrochemical impedance spectroscopy (EIS) and optical analysis of the modified ceria nanostructures revealed an apparent defect-induced reduction in the band gap energy of ceria, resulting in a higher interfacial electron transfer rate and reduced photocarrier recombination under visible light irradiation. The modified ceria nanostructures demonstrated superior photocatalytic activity compared with pristine ceria.[40] In other research, a green method employing an electrochemically active biofilm (EAB) was used to modify ceria nanomaterials and lower their band gaps. The modified ceria nanostructures demonstrated enhanced photoactivity during photoinduced dye degradation compared with pristine ceria.[41−43]

2.2. Oxygen Storage Capacity and Catalytic Properties of Ceria. Ceria is capable of storing oxygen through variation of its stoichiometry, enabling it to supply oxygen when required during oxidation reactions or remove it during reduction reactions.[44] The ability of ceria to act as an "oxygen reservoir" fundamentally arises from the ease with which Ce transitions between its +3 and +4 oxidation states, as illustrated in Figure 1. This redox behavior is critical for most catalytic

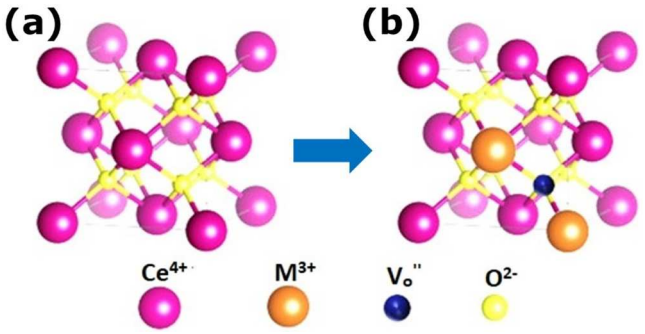

Figure 1. Crystal structures of (a) pure ceria and (b) ceria containing M^{3+} ions and the associated oxygen vacancies.

applications of ceria and is influenced by parameters including the size and shape of ceria NPs. Research has revealed that particles of size <5 nm release more active oxygen than larger NPs.[6] Moreover, particle shapes, such as rods and cubes, tend to exhibit better oxygen storage performance than other polyhedrons, such as octahedrons. This oxygen reservoir property also enables ceria to act as a radical scavenger, thus making it a valuable material in the biomedical field.[45] Compared with materials possessing similar band gaps (ZnO and TiO_2, for example), ceria has a higher oxygen ion mobility and a longer photogenerated charge carrier lifetime, making it superior for certain optical and related applications[46,47] Furthermore, ceria is known to be an active oxygen donor in

https://doi.org/10.1021/acsomega.3c01199
ACS Omega XXXX, XXX, XXX−XXX

certain reactions, including three-way catalytic (TWC) reactions to decompose toxic components of automobile exhaust, water−gas shift (WGS) reactions at low temperature, oxygen permeation membrane systems, oxygen sensors, and fuel cells. The oxygen storage capacity of ceria has also been exploited for solar-driven thermochemical water splitting, which is an extremely promising alternative to solar-driven photoelectrochemical water splitting.[24]

3. DOPED CERIA NANOMATERIALS

Structural modification of ceria through the introduction of dopants is one way to improve its properties for different uses, as this usually leads to a lower band gap and the creation of abundant oxygen vacancies or other catalytically active defects. Ceria is particularly amenable to doping with various types of dopants due to the variable oxidation state of the cerium ions in the ceria lattice, making it possible to introduce dopants that can replace cerium in either the +4 or +3 oxidation state. Figure 2 illustrates the different types of dopants that can be

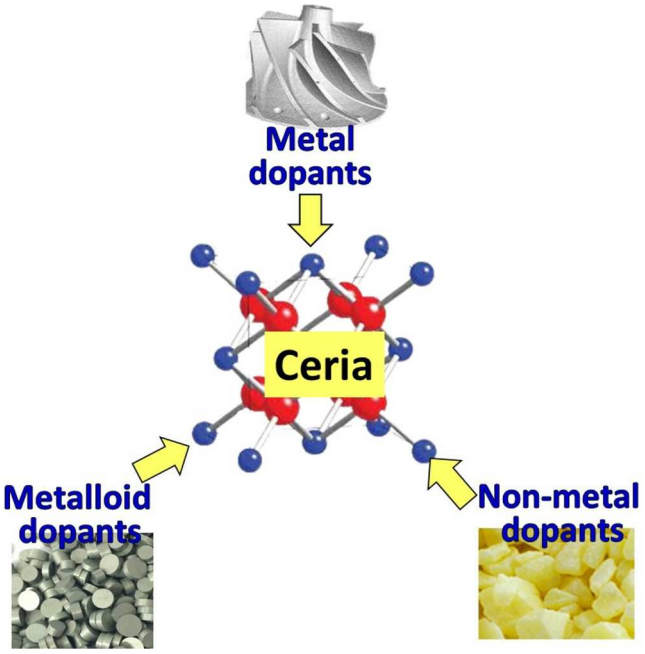

Figure 2. Different types of dopants that have been successfully used to dope ceria.

used for ceria nanomaterials. Doping is a common strategy to modulate the effective conduction band (CB) and/or valence band (VB) energies of semiconductors, as illustrated in Figure 3. For instance, Mn^{2+} doping in the ceria structure induces a shift of the Mn−O antibonding orbitals into the VB, leading to the formation of single spin states at the top of the VB and changing the energy of the VB edge, which in turn leads to enhanced absorption in the visible region.[12] A large number of synthetic methodologies have been reported for doping ceria NPs, including microwave-assisted methods, hydrothermal/solvothermal methods,[48] co-precipitation, microemulsion methods, green synthesis,[49] thermal decomposition,[50] and sol−gel and solid-state synthesis. In this review, the known dopants will be grouped and discussed under the headings metal doped (s, block, d block, and f block elements, and dual/co-doped) and non-metal doped ceria.

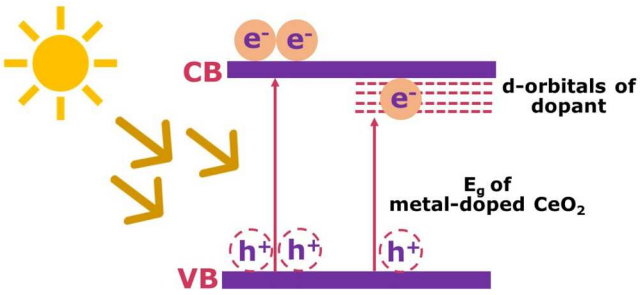

Figure 3. Creation of band gap states and modification of the band gap energy in metal doped ceria.

3.1. Metal Doped Ceria. Metal dopants are known to alter the properties of ceria by increasing the density of oxygen vacancies, thereby extending the range of light absorption into the visible region, which may be useful in optical and photocatalytic applications. Several different groups of metals including s block, d block, and f block elements have been used as dopants in ceria NPs, and these will each be reviewed in the following sections.

3.1.1. s Block Metal Doped Ceria. The s block metals comprise groups 1 (alkali) and 2 (alkali-earth metals) of the periodic table. The doping of ceria with s block metals can alter not only the optical but also the biocidal properties of nanomaterials. The antibacterial activity of ceria NPs arises from the strong reducing and oxidizing agents generated by ceria, which can be controlled by doping with alkaline metal ions. These ions operate as electron traps and lead to changes in the band gap energy, thus slowing down the recombination of electron−hole pairs. In turn, this promotes reactive oxygen species (ROS) production and improves the antibacterial effectiveness of the ceria NPs.[3,7,45,51]

In research conducted by Sisubalan and co-workers, Ba-doped ceria was prepared by the precipitation method, and its biocidal activity was investigated.[45] For comparison, undoped, Mg-doped, Ca-doped, and Sr-doped ceria were also tested. TEM observations revealed that the undoped ceria NPs adopted a spherical structure, while the various types of doped ceria showed needlelike structures with average sizes of 23, 19, 15, 13, and 10 nm for the undoped, Mg-, Ca-, Sr-, and Ba-doped ceria, respectively, with corresponding band gap energy values of 2.85, 2.9, 2.95, 3.0, and 3.1 eV. Radical scavenging activities determined by 2,2-diphenyl-1-picrylhydrazyl (DPPH) assay were 57.4%, 55.9%, 51.7%, 65.5%, and 68.0% for the undoped, Mg-, Ca-, Sr-, and Ba-doped ceria, respectively. The antibacterial results showed that Ba-doped ceria had the highest biocidal activity, and this was attributed to it comprising the smallest particles and exhibiting the highest ROS production rate.[45]

Na-doped ceria prepared via a cryochemical route in liquid nitrogen with different molar ratios of Na and Ce was tested as a catalyst for CO_2 hydrogenation.[52] The results revealed that the yield of CO produced varies with the Na/Ce ratio used. A Na/Ce ratio of 10 resulted in the lowest yield of 2.51 mmol/g_{cat}/h. On increasing the ratio to 100, the performance improved with a yield of 3.90 mmol/g_{cat}/h, but a decline in yield was observed for a higher ratio of 200 (3.72 mmol/g_{cat}/h), indicating that there is an optimum molar Na/Ce ratio that gives the best performance. The catalyst with optimum performance exhibited a lower order of reaction in CO_2 and the highest density of oxygen vacancies in its structure.

https://doi.org/10.1021/acsomega.3c01199
ACS Omega XXXX, XXX, XXX−XXX

In other research, the effect of Na dopant concentration on the activity of a Ni/CeO_2 catalyst for the water−gas shift (WGS) reaction was studied.[53] The CO_2 generated with 2 wt % Na doping corresponds to 97.5% yield, but on increasing the doping to 5 and 10 wt %, the yield decreased to 97.1% and 94.4%, respectively. The result revealed that 2 wt % Na-doped ceria exhibited the best performance as a catalyst for the WGS reaction as well as for suppressing methane generation, which is an unfavorable side reaction. The peak efficiency of this catalyst arose because Na has a solubility limit of 2% in the ceria lattice, at which the optimal oxygen vacancy density is produced. Above this percentage, sodium is no longer incorporated into the ceria structure due to the solute drag effect, which inhibits grain boundary movement, and the oxygen vacancy density in the ceria is no longer optimum. Na-doped ceria has also been investigated as a catalyst for the dehydration of 1,5-pentanediol.[54] The results revealed that the doped ceria was more selective than the undoped ceria, thus, suppressing unwanted side reactions. However, the incorporation of Na into the ceria structure reduces the number of intrinsic defects and, thus, lowers the dehydration rate.

Doped ceria has also been evaluated as a catalyst for organic reactions. In research conducted by Zhou and co-workers, Ca-doped ceria beads were prepared by the cation exchange method and tested for acetic acid ketonization.[18] SEM observations showed that the 6 wt % Ca-doped ceria material had an average diameter of about 40 nm and was more monodisperse than the undoped ceria (average diameter ∼100 nm). The catalytic test performed at 350 °C revealed that the 6 wt % Ca-doped ceria was stable and more selective toward the formation of acetone, while the undoped ceria experienced deactivation leading to a ∼15% drop in conversion. Similarly, the catalytic dehydration of 2-octanol using a Ca-doped ceria catalyst synthesized by thermal decomposition was investigated.[55] The BET surface area values of the catalyst powders were 89, 95, and 100 m^2/g for the undoped and 0.15 wt % and 0.50 wt % Ca-doped ceria powders, respectively; a further increase in doping to 1.25 wt % resulted in a reduction in surface area to 91 m^2/g. SEM showed that the 0.15 wt % Ca-doped ceria comprised smaller and more monodisperse particles than the undoped ceria. The catalytic test revealed that the 0.15 wt % Ca-doped ceria displayed the best performance for the conversion of 2-octanol, while the undoped ceria experienced a 35% drop in conversion after some time. However, for both Ca-doped and undoped ceria, the selectivity of product formation was the same.

Ca-doped ceria has also been investigated as a potential photocatalyst. In research conducted by Ramasamy and co-workers, Ca-doped ceria with various dopant concentrations was prepared by the sol−gel method and tested for the photodegradation of methylene blue.[56] The experiments were performed under solar irradiation in the open, and aliquots were taken at 10 min intervals over a period of 50 min. The photocatalytic efficiencies of undoped and 1, 3, 5, and 7 wt % Ca-doped ceria were 60%, 57%, 76%, 84%, and 78%, respectively. It can be observed that the 5 wt % Ca-doped ceria has the highest photocatalytic response, and this has been attributed to its smaller crystallite size (as calculated from p-XRD) compared to ceria with other dopant concentrations. The smaller size of 5 wt % Ca-doped ceria leads to a higher surface area and thus a greater number of active surface sites per unit mass.

The application of s block metal doped ceria for photocatalytic applications has also been reported by Murugan and co-workers. These authors synthesized group 2 metal (Mg, Ca, Sr, and Ba) doped ceria nanomaterials using a hydrothermal method.[57] The incorporation of these metals into ceria was evident in the Raman spectra as a reduction in the intensity and a shift in the wavenumber of the peaks. The average particle size observed in the TEM images suggested that doping decreases the particle size due to supersaturation effects during particle nucleation and growth, leading to a higher nucleation rate relative to the crystal growth rate. The effect of doping on methylene blue degradation was investigated, and the results revealed that the doped ceria was more effective at degrading MB than undoped ceria, with solution transmittance values after degradation of 43, 79, 86, 89, and 97% recorded for undoped, Mg-doped, Ca-doped, Sr-doped, and Ba-doped, respectively. The synthesis, properties, and applications of s block metal doped ceria are summarized in Table 1.

It is clear from the surveyed literature that s block doped ceria has been synthesized using a range of well-established synthetic methods, namely, co-precipitation, sol−gel, hydrothermal, thermal decomposition, cryochemical, and cation exchange methods. However, certain modern techniques such as microwave-assisted or ultrasound-assisted synthesis have not been explored in detail, and most studies only focus on one or a few dopant metals, which makes it difficult to directly compare the influence of different dopants due to variations in the synthesis method and, consequently, the resultant particle size and morphology. This is particularly critical because most of the surveyed applications of s block metal doped ceria require fine control over not only the metal dopant concentration but also the size and shape of the ceria particles for optimum performance. It is therefore advisable to explore a broader range of synthetic methods to obtain better control over the dopant concentration and ceria particle size and shape. It would also be interesting to conduct more systematic studies covering a wider range of s block dopants to facilitate direct comparisons between s block metal doped ceria prepared using the same synthesis method.

3.1.2. d Block Metal Doped Ceria. The inclusion of less expensive transition metals in the lattice of ceria can enhance heat stability, improve redox properties, and control the density of oxygen vacancies, resulting in superior catalytic activity, which can be attributed to the variable oxidation state of transition metals and the strong synergy that exists between them and ceria. This section summarizes the various transition metals that have been used successfully as dopants for ceria.

Ni-, Fe-, and Mn-doped ceria were prepared using a hydrothermal method and evaluated as catalysts for the oxidative dehydrogenation of ethane.[58] The ceria doped with Ni was more selective toward CO production (94%), and this was attributed to the synergy between Ce and Ni leading to the formation of elemental Ni; thus this reaction was dry reforming rather than selective oxidation, while in Mn-doped ceria, the oxygen was activated, and there was no formation of metallic Mn. Hence, only moderate conversion of ethane (39.7%) and selectivity toward ethylene (45.6%) were achieved. In another work, Mn-, Fe-, Co-, Ni-, and Cu-doped ceria were prepared by the reverse microemulsion method and then tested as catalysts in a fuel cell.[59] SEM revealed different grain sizes for the different dopants, with the largest grain observed for Cu while Ni has the smallest. The electrical tests revealed a decrease in current density, except for Ni- and Co-doped ceria, which were

https://doi.org/10.1021/acsomega.3c01199
ACS Omega XXXX, XXX, XXX−XXX

Table 1. Synthesis, Properties, and Applications of s Block Metal Doped Ceria

material	synthesis method	band gap energy (eV)	morphology	application	performance	ref
Mg-, Ca-, Sr-, and Ba-doped	precipitation	2.85 = undoped ceria; 2.9 = Mg-doped; 2.95 = Ca-doped; 3.0 = Sr-doped; 3.1 = Ba-doped	undoped ceria = spherical; doped ceria = needle-like; particle sizes (in nm): 23 = undoped; 19 = Mg-doped; 15 = Ca-doped; 13 = Sr-doped; 10 = Ba-doped	antibacterial	scavenging activities of 57.4% = undoped ceria; 55.9% = Mg-doped; 51.7% = Ca-doped; 65.5% = Sr-doped; 68.0% = Ba-doped	45
Na-doped	freezing route in liquid N_2	not reported	size less than 10 nm	CO_2 hydrogenation	yield of CO (mmol/g_{cat}/h): Na/Ce of 10 = 2.51; Na/Ce of 100 = 3.90; Na/Ce of 200 = 3.72	52
Na-doped Ni/ceria	wet impregnation method	not reported	15.3 nm = undoped; 23.1 nm = 2% Na-doped; 23.6 nm = 5% Na-doped	WGS reaction	yield of CO_2: 2 wt % Na -doped = 97.5%; 5 wt % Na-doped = 97.1%; 10 wt % Na-doped = 94.4%	53
Ca-doped	gelation/cation exchange	not reported	6 wt % Ca-doped = 40 nm; undoped ceria = 100 nm	acetic acid ketonization	6 wt % Ca-doped = more stable and selective; undoped ceria = deactivated (15% drop conversion)	18
Ca-doped	thermal decomposition	not reported	undoped ceria= polyhedron; 0.15 wt % Ca-doped = cuboid	dehydration of 2-octanol	0.15 wt % Ca-doped = optimum performance; undoped ceria = 35% drop in conversion	55
Ca-doped	sol–gel	not reported	spherical NPs	photodegradation of methylene blue	photocatalytic efficiencies: undoped = 60%; 1 wt % = 57%; 3 wt % = 76%; 5 wt % = 84%; 7 wt % = 78%	56
Na-doped	wet impregnation method	not reported	not reported	dehydration of 1,5-pentanediol	Na-doped ceria = more selective, less % conversion; undoped ceria = less selective, more% conversion	54
Mg-, Ca-, Sr-, and Ba-doped	hydrothermal method	not reported	average size: undoped ceria= 3.25 nm; doped ceria < 3.25 nm	degradation of methylene blue	solution transmittance after degradation: 43% = undoped; 79% = Mg-doped; 86% = Ca-doped; 89% = Sr-doped; 97% = Ba-doped	57

the most stable. The catalytic behavior of Ni- and Co-doped ceria above is in contrast with what was observed when they were prepared by the hydrothermal method and studied as a catalysts in the conversion of toluene by another research group.[60] The temperatures at which 50% of the toluene was converted were 267, 217, 231, 242, and 254 °C for undoped and Cu-, Mn-, Zn-, and Fe-doped ceria, respectively. In contrast, for Ni and Co-doped ceria, 50% conversion of toluene was observed at temperatures as high as 274 and 326 °C, respectively, which is poor compared to that for pure ceria.

The effect of ionic radii on the oxygen storage capacity and electrochemical activity toward hydrogen oxidation in fuel cells was investigated for ceria doped with Ni, Cu, Co, Mn, Ti, and Zr.[61] The results revealed that the Ni- and Cu-doped ceria had a higher oxygen storage capacity. For example, $Ce_{0.7}Cu_{0.3}O_{2-\delta}$ exhibited about 1 mol $[O_2]$/g of oxygen storage capacity and high redox stability at 700 °C. Likewise, $Ce_{0.9}Ni_{0.1}O_{2-\delta}$ generated a power density of 0.15 W/cm^2 when evaluated as an anode in a solid oxide fuel cell. The good performance of these Ni- and Cu-doped ceria was attributed to their smaller ionic radii and lower redox potential.

A comparison between two methods of preparation (co-precipitation and mechanochemical activation) and the resulting WGS activity was studied by Tabakova and co-workers.[62] The results showed that the samples prepared by mechanochemical activation had better catalytic activity than those prepared using co-precipitation. Fe- and Mn-doped ceria prepared by mechanochemical activation displayed the best performance, with Fe-doped ceria experiencing good stability with just a 7% drop in conversion efficiency. The results were justified by the data obtained on both methods of preparation; doped ceria samples prepared by the mechanochemical conversion had a larger fraction of smaller size compared with those prepared by the co-precipitation route as is also evident in the XPS analysis with a high concentration of Ce^{3+} ions present in the Fe- and Mn-doped ceria.

The photocatalytic response of some transition metal doped (Mn^{3+} and Fe^{3+}) ceria was compared with rare earth metal doped (La^{3+} and Pr^{3+}) ceria synthesized by the sol−gel method and studied for the degradation of rhodamine B.[63] The band gap energy values of 3.01, 2.45, 2.77, 2.90, and 2.87 eV were calculated for undoped, Mn-doped, Fe-doped, La-doped, and Pr-doped ceria, respectively. The photoluminescence spectra revealed that there is a red shift and broadening of peaks with doped ceria, and the highest shift was recorded for the Mn-doped ceria. Thus, Mn-doped ceria showed the best photocatalytic response followed by Fe-doped ceria, while the La- and Pr-doped ceria had reduced activity. This has been attributed to the higher surface area and more oxygen vacancies present with the transition metal ions.

Furthermore, the first-row transition metals have been studied more, and their properties have been evaluated in various applications. For instance, Cu-doped ceria was synthesized by thermolysis of a metal−organic framework (MOF) precursor, and the resulting porous nanostructures were tested as a catalyst for CO and NO elimination.[64] The nanostructures were obtained from two different ligands, benzene dicarboxylic acid (BDC) and 4,4-biphenyl dicarboxylic acid (BPDC). The resultant Cu-doped ceria had specific surface areas of 88.11 and 97.00 m^2/g, from BDC and BPDC, respectively. The catalytic results revealed that, for the conversion of CO into CO_2, the conversion temperatures of the two Cu-doped ceria nanostructures are 110 and 140 °C for

https://doi.org/10.1021/acsomega.3c01199
ACS Omega XXXX, XXX, XXX−XXX

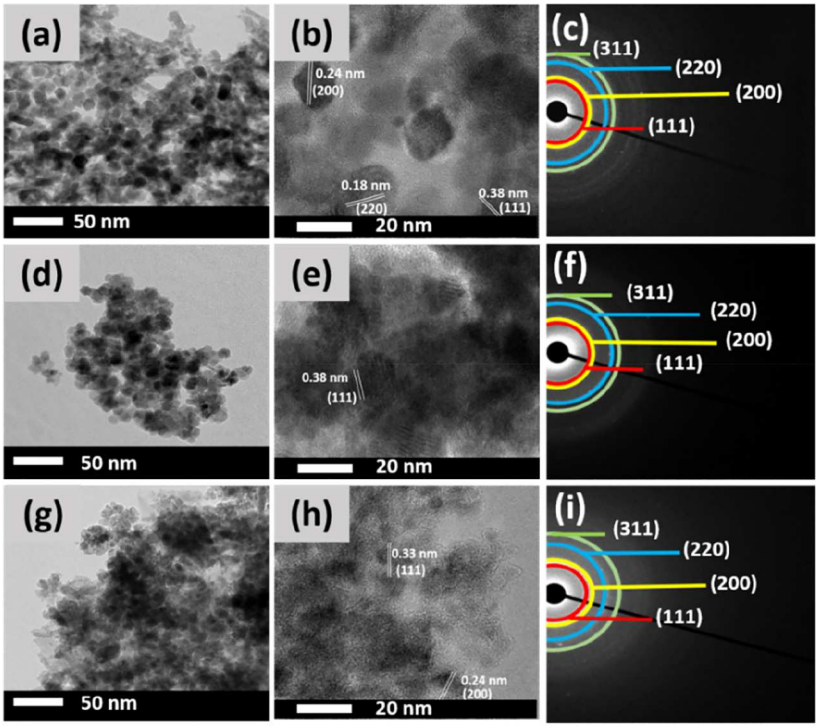

Figure 4. TEM, HR-TEM, and SAED patterns of (a–c) undoped, (d–f) 4% Co-doped, and (g–i) 12% Co-doped ceria NPs. Reproduced from ref 70 under the terms of a Creative Commons CC-BY-4.0 license.

BPDC and BDC, respectively. The better catalytic activity of Cu-doped ceria from BPDC is consistent with its higher surface area.

The effect of different concentrations of Cu-doped ceria synthesized by the hydrothermal method was investigated by Mužina and co-workers.[10] The size decreases with increasing copper concentration from 6 nm (undoped ceria) to 3.8 nm (0.4 mol of Cu-doped ceria). This is also evident in the band gap energy as the values obtained decrease with an increase in Cu concentration. The decrease in the band gap was attributed to the introduction of defect energy states in the band gap, which slows the transition of electrons and eventually results in a narrowing of the band gap. The hydrogen reduction experiment revealed that the reaction temperature decreases while the amount of hydrogen consumed increases with increasing doping; the undoped ceria required 410 °C to reduce 0.26 mmol/g of H_2, while with the 40% Cu-doped ceria, the reaction could be carried out at a low temperature of 141 °C with the consumption of 1.27 mmol/g H_2.

Mn-doped ceria nanomaterials were prepared by the polyol-assisted co-precipitation method, and their catalytic activity was evaluated.[65] The 7% Mn-doped ceria displayed the best catalytic performance compared with that of the undoped ceria and 2 and 4 mol % Mn ion doped catalysts. This efficiency has been attributed to the increase in the charge transport rate. The electrical resistivity of Mn-doped ceria ($Ce_{1-x}Mn_xO_2$) synthesized by the solid-state method was investigated by Kumar and co-workers,[66] whose Raman study revealed a red shift in the peaks at $x = 0.07$, whereas a blue shift was observed for $x = 0.15$. The electrical resistivity measured as a function of temperature showed an increase in resistivity with Mn doping; the room temperature dielectric constant at 2 kHz frequency was found to be about 20 and 53 for undoped ceria and $Ce_{1-0.15}Mn_{0.15}O_2$, respectively. Mn-doped ceria was prepared by co-precipitation, and the UV absorption was studied and compared with undoped ceria.[67] The band gap energy of the Mn-doped ceria is 3.0 eV while that of the undoped ceria is 3.2 eV, and this manifested in their UV absorption, where the Mn-doped ceria demonstrated enhanced absorption compared to that of the pure ceria.

Co-doped ceria was prepared by the precipitation method and was tested as a catalyst in oxidation reactions and as an optical sensor for H_2O_2 detection.[68] The Co-doped ceria exhibited 100% CO and propane conversion at 450 °C with the optimum catalyst loading of 0.75 wt % Co and also exhibited a wide range of detection and a very low detection limit. The application of Co-doped ceria was also extended to the hydrogen evolution reaction. The Co-doped ceria was synthesized by the solvothermal route, and the results showed that the Co-doped ceria nanosheets had the best performance with an overpotential of 132 mV at 100 mA/cm^2 while the undoped ceria has an overpotential of 301 mV at the same current density.[69]

Furthermore, Co-doped ceria of various Co weight percentages was synthesized by microwave-assisted synthesis and investigated for the photocatalytic degradation of methylene blue and 4-nitrophenol.[70] TEM measurements revealed particle sizes between 4 and 13 nm (Figure 4), while the band gap energy values obtained were 2.56, 2.46, 2.41, 2.32, and 2.28 eV for the undoped and 1%, 4%, 8%, and 12% doped ceria, respectively. The results from the photocatalytic degradation experiments showed that the 12% Co-doped ceria exhibited the best performance due to its lower band gap energy.

The green synthesis method has been used for Ni-doped ceria and its UV protection was evaluated.[49] The findings indicated that increasing the concentration of Ni doping enhanced the activity as observed in the sun protection values;

https://doi.org/10.1021/acsomega.3c01199
ACS Omega XXXX, XXX, XXX−XXX

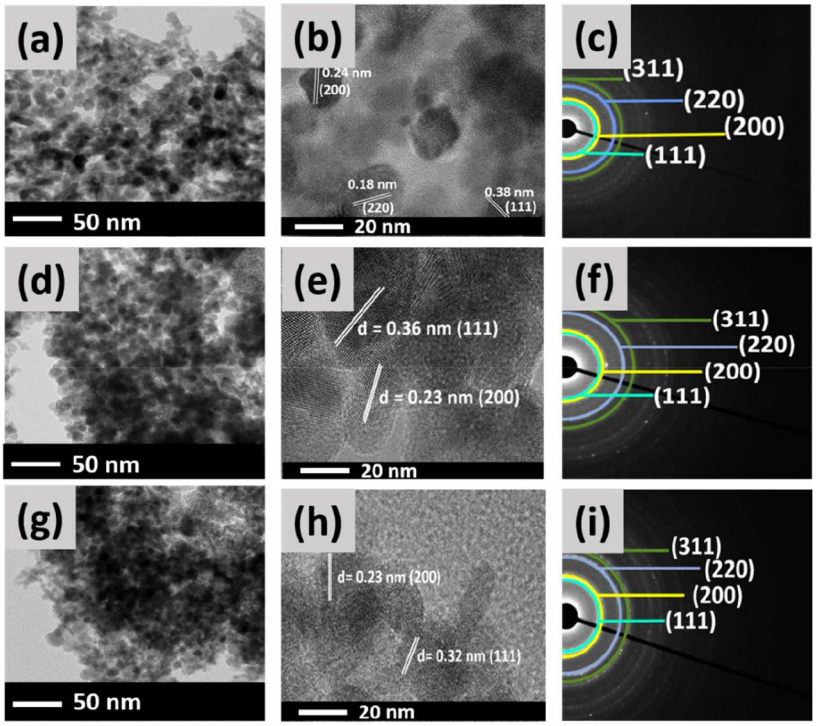

Figure 5. TEM, HR-TEM, and SAED patterns of (a–c) undoped, (d–f) 0.5% Pd-doped, and (g–i) 5% Pd-doped ceria NPs. Reproduced from ref 82 under the terms of a Creative Commons CC-BY-4.0 license.

40.9, 43.6, 46.6, and 48.5 were recorded for the undoped ceria and 1%, 3%, and 5% Ni-doped ceria, respectively. In other work, Ni-doped ceria's reducibility performance was compared with that of nickel deposited over ceria as support.[50] The decomposition of a Schiff base complex was used to produce Ni-doped ceria, and the result revealed that the Ni-doped ceria performed 7 times better than the one used as support.

Fe-doped ceria was prepared by co-precipitation, and its specific capacitance was investigated.[71] The 10% Fe-doped ceria exhibited excellent cycling stability and a high specific capacitance of 559 F/g, while the undoped ceria gave ∼121 F/g at 1 A/g. The anticancer activity of Fe-doped ceria synthesized by the green method has also been studied by Rahdar and co-workers.[72] A half-maximal inhibitory concentration (IC_{50}) of 6.1 and 3.02 mg/mL was recorded for the Fe-doped ceria NPs after 48 and 72 h exposure, respectively, and it is noteworthy that cancer cell viability was reduced to about 21% within 72 h of exposure to the Fe-doped ceria. The colorimetric detection of 2,4-dinitrophenol at a low detection limit of 0.45 μg/mL was also achieved using a polymeric Fe-doped ceria incorporated into Au NPs to form a support.[73]

The effect of the ratio of Ce to Cr on the catalytic performance was studied by Venkataswamy and co-workers.[74] The Cr-doped nanomaterials were prepared by the hydrothermal method in 3 different Cr percentages of 5%, 10%, and 15%. The energy band gap values revealed an initial decrease in band gap from 2.93 eV for undoped to 2.73 eV for 5% Cr-doped and 2.64 eV for 10% Cr-doped but on increasing the doping to 15%, the value rose to 2.82 eV. The 10% Cr-doped exhibited the best catalytic performance with the lowest oxidation temperature of 261 °C, followed by 5% doped (286 °C), 15% doped (303 °C), and undoped ceria (338 °C). The efficiency of the 10% Cr-doped ceria was attributed to its high oxygen vacancy concentration and surface area, as is evident from XPS and BET analysis.

V-doped ceria has been synthesized by the calcination of sol and tested as a catalyst in syngas production.[75] The average particle size increased from 18 nm for undoped ceria to 38 nm for the 7% V-doped ceria, and an increase in porosity was also observed. The syngas production increased with V-doped ceria with the production of about 90 mmol/g of the gas, while the activation temperature decreased from 962 °C in undoped ceria to 784 °C in V-doped ceria.

A simple co-precipitation method utilizing the green reagent oxalic acid was used to produce Zn-doped ceria.[76] The band gap energy of ceria NPs is ∼3.09 eV, and that of Zn-doped ceria is ∼3.12 eV. The difference in the band gap can mainly be attributed to quantum confinement in the smaller Zn-doped particles, which increases the band gap energy. Other transition metals, such as cadmium, have also been used to dope ceria. Ramasamy and co-workers prepared Cd-doped ceria by co-precipitation, and the optical properties were investigated.[77] The band gap energy was found to increase with decreasing particle size, which led to improved absorption in the visible region. The doped ceria with the best optical behavior is that with 0.4 wt % Cd with weaker intensity peaks and red shift observed in its photoluminescence spectrum confirming its higher oxygen vacancies.

Diverse applications resulting from doping ceria with the second- and third-row d block elements have also been reported by many research groups.[12,51,78,79] For instance, Zr-doped ceria was prepared using a biosynthetic route, and the antibacterial activities were evaluated.[51] A reduction in band gap energy value was observed with increasing % doping; the calculated values are 2.64, 2.60, 2.55, and 2.54 eV for the undoped ceria and 1% Zr-, 5% Zr-, and 10% Zr-doped ceria, respectively. The bactericidal tests showed growth inhibition

https://doi.org/10.1021/acsomega.3c01199
ACS Omega XXXX, XXX, XXX−XXX

and cell death at a concentration of 1024 μg/mL for undoped ceria and a concentration of 512 μg/mL for 1% Zr-doped ceria. Interestingly, a reduction in bactericidal activity was found for 5% and 10% Zr-doped ceria. Similarly, Ag-doped ceria was produced by the biosynthesis method, and its cytotoxicity was investigated using the electromagnetic perceptive gene (EPG) human gastric cancer cell line, and it showed no significant cytotoxicity for concentrations up to 62.5 mM.[78]

Furthermore, the photodegradation activities of Ag-, Au-, and Pt-doped ceria synthesized by the hydrothermal method have been evaluated.[79] Their band gap energy values are 2.57, 2.32, 2.20, and 2.18 for the undoped ceria and Au-doped, Ag-doped, and Pt-doped, respectively. The catalyst Au-doped ceria is the most active, having a degradation efficiency greater than 98%. In another study, the photocatalytic reduction of CO_2 using Mo-, Y-, and La-doped ceria prepared by the hydrothermal method was investigated.[12] The Y-doped ceria had the best performance, producing 22 ppm of CO gas in the first hour, followed by Mo-doped with 8 ppm of CO generated in the first 3 h.

Pd-doped ceria NPs have also been investigated for various applications. In research conducted by Liu and co-workers, Pd-doped ceria prepared by the hydrothermal method was used for the electrochemical detection of phenol.[80] The Pd-doped ceria sample with 5% doping gave the best result with good thermal stability and a detection limit of 0.39 μmol/L. In other research, the cytotoxicity of PEGylated Pd-doped ceria was compared with Pd NPs and ordinary Pd-doped ceria.[81] These were tested on a human lung cancer cell line, and the findings revealed that the PEGylated Pd-doped ceria exhibited strong cytotoxicity with an IC_{50} ∼ 81.25 μg/mL, followed by Pd-doped ceria (∼118.75 μg/mL), and last, ∼231.25 μg/mL was observed for Pd NPs.

Pd-doped and undoped ceria NPs of different Pd weight percentages (0.5%, 1%, 3%, and 5%) were synthesized via the microwave-assisted synthesis method.[82] Mixed phases of CeO_2/Ce_2O_3 were observed in undoped ceria (S-CeO_2) and Pd-doped ceria, but the Ce_2O_3 phase gradually disappeared upon doping with higher amounts of Pd. TEM observations revealed that almost spherical particles were obtained with average sizes between 6 and 13 nm, with the particle size decreasing as more Pd was added (Figure 5). The band gap energy values were 2.56, 2.50, 2.47, 2.42, and 2.27 eV for the undoped ceria and 0.5%, 1%, 3%, and 5% Pd-doped ceria NPs, respectively. The photocatalytic degradation, photoelectrochemical, and photo-antibacterial activities of the ceria NPs under visible light irradiation were all improved after Pd doping. The 1% Pd-doped ceria NPs showed the best activity toward the photocatalytic degradation of methylene blue, which was attributed to optimal Pd loading. Thus, further increases in doping did not enhance the degradation of methylene blue. Table 2 summarizes the recent work on d block metal doped ceria and its various applications and related findings.

It is evident from the above reports that d block metal doping of ceria has been studied more extensively than doping with s block metals, and a wider range of synthetic routes have been utilized. In general, doping with an optimized amount of d block metal tends to decrease the band gap energy of ceria due to the contribution of the metal d-orbitals to the ceria conduction band. This lowering of the band gap makes d block metal doped ceria particularly useful in photocatalytic applications, where absorption of low-energy photons in the visible portion of the solar spectrum is desirable to maximize light harvesting. The performance of the doped ceria is also influenced by the morphology of the NPs obtained, which, in turn, depends on the synthetic route employed. In most studies, only one or at most a few dopant metals are examined, and it is therefore difficult to make direct comparisons between different dopants due to differences in experimental conditions or the size and shape of the resulting ceria particles. It is therefore recommended that more systematic studies comparing different dopants be performed, with the aim of isolating the influence of the metal dopant on the intrinsic properties of the ceria and deconvoluting it from effects simply arising from variations in the particle size and shape.

3.1.3. p Block Metal Doped Ceria. Tin (Sn) is one of the popular p block metals that is used in doping ceria because it has a smaller radius and thus can be easily incorporated into the ceria structure. In research conducted by Naidi and co-workers, Sn-doped ceria of different dopant percentages was synthesized by the green method and tested for its photo-antioxidant properties.[3] The band gap energy values obtained are 2.66, 2.47, 2.53, and 2.58 eV for undoped ceria, 1% doped, 5% doped, and 10% doped, respectively. A study of photo-antioxidant properties revealed no dose effect under dark conditions, and the radical scavenging activity (RSA) was improved in all cases when subjected to visible light irradiation. The 1% Sn-doped ceria exhibited the highest scavenging efficiency, while the undoped ceria had the least activity, and this was attributed to their band gap energy; the undoped ceria has the highest value, while the 1% Sn-doped ceria had the lowest value. Furthermore, Sn-doped ceria was prepared by the precipitation method and tested as an electrochemical sensor for nitrites in water.[83] The Sn-doped ceria particles had a spherical shape and an average diameter of 8.5 nm and were highly sensitive toward nitrite ions, exhibiting excellent electrocatalytic oxidation of NO_2^- and a very low detection limit of 16 nM.

Bi-doped ceria supported gold NPs were investigated for the oxidation of alcohols. The efficiency of the catalyst depends on optimizing the concentration of Bi and Au with 3.5 wt % Au/6 mol % Bi exhibiting the best performance in oxidizing benzyl alcohol to benzaldehyde. A high selectivity of 99% was recorded with 60% conversion. A high turnover frequency value of 0.14/s was recorded and the better performance of this catalyst was attributed to its small size, higher oxygen vacancy sites, and more positively charged Au particles.[84] Table 3 shows the p block metal doped ceria and their applications and respective findings.

3.1.4. f Block Metal Doped Ceria. Doping ceria with f block elements with low activation energies for vacancy formation is a feasible method of enhancing the catalytic activity and ionic conductivity of ceria.[85] The conductivity of Sm/Gd co-doped ceria prepared by the precipitation method was investigated by Kannan and co-workers.[86] The conductivity results revealed that the co-doped ceria demonstrated higher conductivity at higher temperatures, and this was explained by the fact that when the Ce^{4+} is substituted by the Gd ion, it leads to the creation of oxygen vacancies and thus a reduced activation energy and higher conductivity. Furthermore, samarium-doped ceria was synthesized by the hydrothermal method with varied percentages of dopants and then tested for its catalytic activity toward CO oxidation.[87] SEM showed that as the percentage of doping increases, the morphology becomes more defined. The catalytic evaluation revealed that the Sm-doped ceria had

https://doi.org/10.1021/acsomega.3c01199
ACS Omega XXXX, XXX, XXX−XXX

Table 2. Synthesis, Properties, and Applications of d Block Metal Doped Ceria

material	synthesis method	band gap energy (eV)	morphology	application	performance	ref
Cu-doped	thermolysis of MOF	not reported	nanorods and nanobundles	conversion of CO into CO_2	conversion temperatures prepared from different ligands are 110 °C = 4,4-biphenyldicarboxylic acid and 140 °C = benzenedicarboxylic acid	64
Ni-, Fe-, and Mn-doped	hydrothermal	not reported	nanorod = undoped ceria; nanorod = Mn-doped ceria; nanoribbon = Fe-doped	dehydrogenation of ethane	Ni-doped was selective to CO production (94%); Mn-doped: 39.7% = ethane conversion, 45.6% = ethylene selectivity	58
Mn-, Fe-, Co-, Ni-, and Cu-doped	reverse microemulsion	not reported	porous material	fuel cell	Ni- and Co-doped ceria were the most stable	59
Cu-, Mn-, Zn-, Fe-, Ni-, and Co-doped	hydrothermal	not reported	roughly spherical with sizes 6.1 nm = undoped ceria; 6.3 nm = Mn-doped; 5.8 nm = Cu-doped; 4.2 nm = Zn-doped	conversion of toluene	temperatures corresponding to 50% conversion of toluene are 217 °C = Cu-doped; 231 °C = Mn-doped; 242 °C = Zn-doped; 254 °C = Fe-doped; 274 °C = Ni-doped; 326 °C = Co-doped; 267 °C = undoped ceria	60
Mn-doped	co-precipitation	3.0 = Mn-doped; 3.2 = undoped ceria	8 nm = Mn-doped; 12 nm = undoped	optical	Mn-doped ceria showed enhanced absorption compared with pure ceria	67
Ni-, Cu-, Co-, Mn-, Ti-, and Zr-doped	calcination	not reported	not reported	redox and electrical conductivity	$Ce_{0.7}Cu_{0.3}O_{2-\delta}$ = oxygen storage 1015 mmol[O_2]/g; $Ce_{0.9}Ni_{0.1}O_{2-\delta}$ = power density 0.15 W/cm^2	61
Fe-, Mn-, and Sn-doped ceria/Au	co-precipitation (CP) and mechanochemical activation (MA)	not reported	sample from MA = 0.5−1.5 nm; sample from CP= 2.5 nm	WGS activity	samples from MA method better than CP; Fe-doped ceria very stable; only 7% drop in conversion efficiency	62
Mn-, Fe-, La-, and Pr-doped	sol−gel	3.01 = undoped; 2.45 = Mn-doped; 2.77 = Fe-doped; 2.90 = La-doped; 2.87 = Pr-doped	undoped ceria = quasi-spherical, 12−14 nm; doped ceria = spherical, 4−8 nm	photocatalytic degradation of methylene blue	photocatalytic responses in order: Mn-doped > Fe-doped > La-doped ∼ Pr-doped	63
Cu-doped	hydrothermal	2.97 = undoped; 2.83 = 10% doped; 2.75 = 20% doped; 2.76 = 30% doped; 2.71 = 40% doped	6.0 nm = undoped ceria; 4.9 nm = 10% doped; 4.3 nm = 20% doped; 4.2 nm = 30% doped; 3.8 nm = 40% doped	catalysis	consumption of H_2: undoped ceria = 410 °C to reduce 0.26 mmol/g; 40% doped = 141 °C to reduce 1.27 mmol/g	10
Mn-doped	co-precipitation	3.13 = undoped; 2.36 = 2% doped; 2.37 = 4% doped; 2.88 = 7% doped	doped ceria = spherical, 10−18 nm	catalysis	7% doped had the best performance	65
Mn-doped	solid state	not reported	undoped = 127 nm; 3% doped = 109 nm; 7% doped = 101 nm	electrical resistivity	dielectric constant at 2 kHz: 20 = undoped ceria; 53 = $Ce_{1-0.15}Mn_{0.15}O_2$	66
Co-doped	precipitation	not reported	spherical NPs, size decreases with increasing doping percentage.	oxidation and as an optical sensor for H_2O_2	Co-doped ceria exhibited 100% CO and propane conversion at 450 °C	68
Co-doped	solvothermal	not reported	nanosheet	HER	overpotential at 100 mA/cm^2: Co-doped = 132 mV undoped ceria = 301 mV	69
Co-doped	microwave-assisted	2.56 = undoped; 2.46 = 1%; 2.41 = 4%; 2.32 = 8%; 2.28 = 12%	irregular pentagonal morphology	photocatalytic degradation of methylene blue and 4-nitrophenol	12% Co-doped ceria showed best response in both photocatalysis reactions	70
Ni-doped	green	not reported	spherical NPs, size decreases with increasing doping percentage	UV protection	sun protection values: 40.9 = undoped ceria; 43.6 = 1% doped; 46.6 = 3% doped; 48.5 = 5% doped	49
Ni-doped	thermal decomposition	not reported	Ni-doped ceria showed truncated octahedra	H_2 reduction	Ni-doped ceria = 7 times better than Ni ceria support	50
Fe-doped	co-precipitation	not reported	nearly spherical NPs undoped = 34 nm; Fe-doped = 32 nm	pseudo-capacitor	specific capacitance at 1 A/g: 10% doped= 559 F/g; undoped ceria = 121 F/g	71
Fe-doped	green	not reported	Fe-doped = spheres with average size of about 26 nm	anticancer	IC_{50} value: 6.1 mg/mL after 48 h; 3.02 mg/mL after 72 h	72
Fe-doped ceria/Au	thermal decomposition	not reported	polymer Fe-doped ceria/Au = spheres of about 8 nm	colorimetric detection of 2,4-dinitrophenol	lower detection limit of 0.45 μg/mL	73
Cr-doped	hydrothermal	2.93 = undoped; 2.73 = 5% doped; 2.64 = 10% doped; 2.82 = 15% doped	nanorods: undoped= 10−15 nm diameter; Cr-doped= 5 nm diameter	CO oxidation	oxidation temperature: 261 °C = 10% doped; 286 °C = 5% doped; 303 °C = 15% doped; 338 °C = undoped	74
V-doped	calcination	not reported	undoped ceria = 18 nm; V-doped = 38 nm	syngas production	activation temperature: 784 °C = V doped; 962 °C = undoped	75
Zn-doped	co-precipitation	3.09 = undoped; 3.12 = Zn doped	clustered cubic NPs	optical	improved absorbance for Zn doped	76

https://doi.org/10.1021/acsomega.3c01199
ACS Omega XXXX, XXX, XXX−XXX

Table 2. continued

material	synthesis method	band gap energy (eV)	morphology	application	performance	ref
Cd-doped	co-precipitation	3.07 = undoped; 3.37 = 0.1 wt %; 3.51 = 0.2 wt %; 3.56 = 0.3 wt %; 3.24 = 0.4 wt %; 3.28 = 0.5 wt %	0.4 wt % Cd-doped = irregular spheres of size 6−7 nm	optical	0.4 wt % doped had the best performance	77
Zr-doped	biosynthesis	2.64 = undoped; 2.60 = 1% doped; 2.55 = 5% doped; 2.54 = 10% doped	undoped ceria = 17 nm; 1% doped = 13 nm; 5% doped = 16 nm; 10% doped = 22 nm	antibacterial	killing properties at: 1024 μg/mL = undoped ceria; 512 μg/mL = 1% doped	51
Ag-doped	biosynthesis	not reported	undoped ceria = 19 nm; Ag-doped average size = 62 nm	cytotoxicity	cytotoxic effects above 62.5 mM	78
Ag-, Au-, and Pt-doped	hydrothermal	2.57 = undoped; 2.32 = Au-doped; 2.20 = Ag-doped; 2.18 = Pt-doped	not reported	photodegradation	Au-doped ceria is most active with efficiency >98%	79
Mo-, Y-, and La-doped	hydrothermal	not reported	doped ceria <20 nm	photocatalytic CO_2 reduction	CO gas produced: Y-doped = 22 ppm in the 1st 1 h; Mo-doped = 8 ppm in the first 3 h	12
Pd-doped	hydrothermal	not reported	undoped ceria = nanorod; Pd-doped = fewer nanorods, more nanocubes	electrochemical detection of phenol	5% Pd-doped has a detection limit of 0.39 μmmol/L	80
Pd-doped/PEG	biosynthesis	not reported	spherical and polydisperse Pd-doped NPs	anticancer	IC_{50}: 81 μg/mL = Pd-doped/PEG; 119 μg/mL = Pd-doped; 231 μg/mL = Pd NPs	81
Pd-doped	microwave-assisted	2.56 = undoped; 2.50 = 0.5% Pd; 2.47 = 1.0% Pd; 2.42 = 3.0% Pd; 2.27 = 5.0% Pd	almost spherical	photocatalytic degradation of methylene blue	photocatalytic responses in order: 1.0% Pd > 5.0% Pd > undoped ceria >0.5% Pd > 3.0% Pd	82

better performance with at least 70% conversion, while the undoped ceria barely reached 40% conversion. The optimal catalyst, $Ce_{0.76}Sm_{0.24}O_2$, was able to convert at 100% because of its higher surface area, as was revealed by Raman spectroscopy, with the most lattice defects.

The role of the precursor in the formation of Sm-doped ceria synthesized by the solid microwave synthesis method was studied by Bregman and co-workers.[88] The investigation revealed that uniform spherical-shaped NPs were formed following the single-step decomposition of cerium tri(methylsilyl) amide (TMA) and samarium tri(methylsilyl) amide while the other precursors such as nitrate and acetate produced nonuniform shapes and sizes. In another report, Sm-doped ceria was synthesized by the thermal decomposition method, and the 15 mol % Sm-doped material had the highest conductivity. This can be explained by the EXAFS results, which revealed that Sm^{3+} ions replaced the Ce^{4+} ions.[89]

The effect of the synthesis method on the structural properties and activity toward soot oxidation for gadolinium-doped ceria was studied by comparing the solvothermal and citrate method.[90] Their band gap energies were calculated to be 3.13 and 2.99 eV for the solvothermal and citrate methods, respectively. The results revealed that the Gd-doped ceria prepared from the citrate method exhibited better performance with a T_{50} value of 468 °C, while the ceria produced by a solvothermal method had a T_{50} value of 500 °C. The better performance of Gd-doped ceria from the citrate method has been attributed to its lower band gap energy and high surface oxygen as seen in the XPS analysis.

Gd-doped ceria has also been extended to use as a contrast agent in MRI. The $Ce_{0.9}Gd_{0.1}O_{1.95}$ nanomaterials prepared by co-precipitation showed the most colloidal stability and a high relaxivity of 3.6 mM^{-1} s^{-1}.[91] In order to improve the performance of the catalyst in fuel cells, Pt nanorods were included on Gd-doped ceria prepared by a flame oxide method. The performance as an oxygen reduction catalyst showed that side reactions are not favored as the catalysts generate less H_2O_2 and are very stable with minimal degradation.[92]

Eu- and La-doped ceria were prepared by the hydrothermal method, and their gas sensing toward CO was investigated.[93] A reduction in the band gap energy of the doped ceria was observed; the undoped ceria had a band gap value of 3.10 eV, while 2.93 and 3.00 eV band gaps were obtained for Eu-doped and La-doped ceria, respectively. Blue-shifted photoluminescence was observed for the La-doped ceria, while a red shift was observed for the Eu dopant. The Eu-doped ceria was the most responsive for carbon monoxide gas sensing, with a very fast response time of only 1 s, compared to those of La-doped (4.2 s) and undoped ceria (6.6 s).

The optical properties of Eu-doped ceria have also been investigated.[94] In research conducted by Sahoo and co-workers, the effect of the percentage doping on the optical properties of Eu-doped ceria prepared by a hydrothermal method was studied, and the band gap energies calculated for the undoped ceria and 0.25, 0.5, 1, and 2 mol % Eu-doped ceria are 3.6, 2.75, 2.75, 2.75, and 3.25 eV, respectively.[95] The photoluminescence spectra showed a red shift for the doped ceria, and this was explained by the existence of defects due to the charge transfer between Ce^{3+} and Ce^{4+} ions. Furthermore, Eu-doped ceria prepared by the precipitation method was used for the detection of sulfite through the chemiluminescence

https://doi.org/10.1021/acsomega.3c01199
ACS Omega XXXX, XXX, XXX−XXX

Table 3. Synthesis, Properties, and Applications of p Block Metal Doped Ceria

material	synthesis method	band gap energy (eV)	morphology	application	performance	ref
Sn-doped	green	2.66 = undoped; 2.47 = 1% doped; 2.53 = 5% doped; 2.58 = 10% doped	spherical NPs with average size 15−20 nm	photoantioxidant	1% Sn-doped = the highest scavenging efficiency; undoped ceria = the least activity	3
Sn-doped	precipitation	not reported	spherical NPs with size 8.5 nm	electrochemical NO_2^- sensor	lower detection limit of 16 nM	83
Bi-doped	sol−gel	not reported	hemispherical	oxidation of alcohol	Bi-doped ceria/Au with 3.5 wt % Au/6 mol % had a selectivity of 99% and 60% conversion	84

energy transfer mechanism.[96] The results showed a very rapid response time of 1 s and a detection limit of 0.007 μM.

The effect of doping on magnetism was also been studied. Tb-doped ceria was prepared by the hydrothermal method with different doping amounts.[97] The band gap energy showed a reduction from 2.61 eV (undoped ceria) to 1.64 eV for Tb-doped. Zn- and Zr-doped ceria were also prepared, but Tb-doped ceria produced the highest fraction of oxygen vacancies (36.85%) because of the dual oxidation states of Tb^{3+} and Tb^{4+}. The Tb-doped ceria nanorods exhibited magnetizations of 0.605 1.089, and 1.489 emu/g for $Ce_{0.9}Tb_{0.1}O_2$, $Ce_{0.8}Tb_{0.2}O_2$, and $Ce_{0.7}Tb_{0.3}O_2$, respectively. These results suggest that magnetization is enhanced as the doping amount increases, which also correlates with the fact that the oxygen vacancies increase with doping.

Similarly, the magnetic properties of La-doped ceria prepared by calcination were studied by Chahal and co-workers.[98] A saturation magnetization value of 0.9×10^{-3} emu/g was recorded for pure ceria, while a significant improvement was observed for the 8% La-doped ceria with a value of 19.6×10^{-3} emu/g. The La-doped ceria had a lower band gap energy (3.08 eV) compared to the undoped ceria (3.21 eV). The photocatalytic test conducted on the La-doped ceria revealed that the 8% La-doped ceria exhibited the highest degradation efficiency of about 87% owing to its oxygen vacancies. On the contrary, Pr-doped ceria prepared by the microwave-assisted method did not show any significant change with Pr dopant concentration; all are superparamagnetic below the blocking temperature of 20 K and paramagnetic above the blocking temperature.[99] Table 4 shows the f block metal doped ceria and their application and respective findings.

3.1.5. Dual- or Co-doped Ceria. Heterometal doping (co-doping or dual doping) can impart very high ionic and electronic conductivity as well as good catalytic activity on doped ceria nanomaterials, which could be useful for diversified applications such as high power production.[86] The approach of co-doping has been used to overcome issues with mechanical stability and also to enhance the ionic conductivity of ceria. Such co-doping is usually achieved by choosing two dopants: one with a smaller radius and the other with a larger radius than ceria. This eventually leads to the expansion and contraction of the ceria structure, thereby enhancing its conductivity.

Sandhya and co-workers investigated the effect of Sb^{3+} and Bi^{3+} radii on the conductivity of ceria.[100] The co-doped ceria was synthesized by co-precipitation, and the results obtained showed that oxygen vacancies were introduced into the ceria structure due to the replacement of Ce^{4+} by the larger Bi^{3+} which led to an increase in the electrical conductivity of the co-doped compared to the undoped ceria as confirmed by the electrochemical impedance measurements. The conductivity value (S cm^{-1}) recorded for single-metal doped $Ce_{0.8}Sm_{0.2}O_{2-\delta}$ was 2.66×10^{-3}, while those of dual-doped $Ce_{0.8}Sm_{0.1}Sb_{0.1}O_{2-\delta}$ and $Ce_{0.8}Sm_{0.1}Bi_{0.1}O_{2-\delta}$ were 3.77×10^{-5} and 3.18×10^{-3}, respectively.

Furthermore, transition metal co-catalysts of Mn/Fe-, Cu/Ag-, Fe/Cu-, and Mn/Cu-doped ceria were synthesized by a hydrothermal method.[48] The band gap energy calculated values are 2.98 eV for Mn/Fe-, 3.09 eV for Cu/Ag-, 2.35 eV for Fe/Cu-, and 2.26 eV for Mn/Cu-doped ceria. The Mn/Cu-doped ceria showed the best catalytic activity for the reduction of exhaust emissions, and this has been attributed to its smallest size and high surface area with more oxygen vacancies.

Green synthesis has also been used to prepare co-doped ceria nanomaterials. For instance, Zr/Sn co-doped ceria have been prepared using an aqueous leaf extract of *Pometia pinnata*, and the photo-antioxidant activities of different co-dopant percentages were investigated.[15] The band gap energy of the 1% Zr/Sn dual-doped ceria was lowered to 2.58 eV from 2.66 eV (undoped ceria). On increasing the concentration to 5%, a further decrease was observed (2.49 eV). However, at 10% doping, the band gap energy increased to 2.54 eV. This has been explained by the difference in the sizes of the cations; thus increased substitution of Ce^{4+} by smaller ions generated oxygen vacancies, which can restrict the movement of oxygen in the structure leading to defect formation. The photo-antioxidant activities of the synthesized materials exhibited better responses under irradiation by visible light compared to dark conditions in terms of both dose- and time-dependent characteristics. The ceria NPs demonstrated significant and concentration-dependent activity against biofilms of Gram-positive bacteria, including *Listeria monocytogenes* and *Staphylococcus aureus*. The highly doped ceria (10% Zr/Sn) inhibited biofilm formation and exhibited antibacterial activity.

The f block elements have also been used as co-dopants for ceria-based materials in different applications.[86] For instance, oxygen-deficient ceria was synthesized by precipitation with co-doping of Sm and Nd followed by sintering at higher temperatures.[101] The obtained material exhibited a large electrorestrictive coefficient of above 10^{-17} $(m/V)^2$ at a low frequency. A summary of dual metal doped ceria and their applications is presented in Table 5.

Overall, very little work has been done on the preparation and applications of dual-doped ceria, especially compared with the volume of work reported for single metal doped ceria. In the literature surveyed above, less than ten dopant combinations are reported, and only four synthetic routes were used to achieve the dual-doped ceria. Nevertheless, these initial reports of dual-doped ceria in conventional heterogeneous catalysis and photocatalysis are very promising, indicating that dual doping may be an important strategy for overcoming the limitations of single metal doping. In view of this, other synthetic routes to dual-doped ceria should be explored with

https://doi.org/10.1021/acsomega.3c01199
ACS Omega XXXX, XXX, XXX−XXX

Table 4. Synthesis, Properties, and Applications of f Block Metal Doped Ceria

material	synthesis method	band gap energy (eV)	morphology	application	performance	ref
Sm- and Gd-doped	precipitation	not reported	grain size 40−70 nm	conductivity	better conductivity at higher temperatures	86
Eu- and La-doped	hydrothermal	3.10 = undoped; 2.93 = Eu-doped; 3.00 = La-doped	spherical NPs of about 4 nm	CO gas sensor	time to sense CO gas: Eu-doped = 1 s; La-doped = 4.2 s; undoped ceria = 6.6 s	93
Sm-doped	hydrothermal	not reported	spherical NPs, smaller size with increasing doping	CO oxidation	optimal catalyst $Ce_{0.76}Sm_{0.24}O_2$ = 100% conversion; undoped ceria = 40% conversion.	87
Tb-doped	hydrothermal	2.61 = undoped ceria; 1.64 = Tb-doped	nanorods	magnetic	saturation magnetization values: 0.605 emu/g = $Ce_{0.9}Tb_{0.1}O_2$; 1.089 emu/g = $Ce_{0.8}Tb_{0.2}O_2$; 1.489 emu/g = $Ce_{0.7}Tb_{0.3}O_2$	97
Sm-doped	solid microwave	not reported	spherical NPs	decomposition pattern	uniform morphology with TMA; nitrate and acetate produced nonuniform morphology	88
Sm-doped	thermal decomposition	not reported	shapes become more irregular with increasing temperature	ionic conductivity	15 mol % Sm-doped had the highest conductivity	89
Gd-doped	solvothermal/ citrate	3.13 = solvothermal; 2.99 = citrate	spherical = citrate; agglomerated = solvothermal	soot oxidation	T_{50} value: 468 °C = citrate method; 500 °C = solvothermal method	90
Gd-doped	co-precipitation	not reported	size of about 2 nm	MRI contrast agent	$Ce_{0.9}Gd_{0.1}O_{1.95}$ has a relaxivity of 3.6 mM^{-1} s^{-1}	91
Gd-doped/ Pt	flame oxide	not reported	polyhedral shape Gd-doped ceria	ORR	less side reaction producing H_2O_2	92
Eu-doped	hydrothermal	undoped ceria = 3.6; 0.25% = 2.75; 0.5% = 2.75; 1% = 2.75; 2% = 3.25	undoped ceria= cubic shape; Eu-doped= irregular shape	optical	red-shifted PL peaks for doped ceria	95
Eu-doped	co-precipitation	not reported	spherical shape with sizes in range 4−6 nm	detection of sulfite	rapid response time of 1 s; detection limit of 0.007 μM	96
Tb-doped	hydrothermal	2.61 = undoped; 1.64 = Tb-doped	nanorods	magnetic	magnetization values: 0.605 emu/g = $Ce_{0.9}Tb_{0.1}O_2$; 1.089 emu/g = $Ce_{0.8}Tb_{0.2}O_2$; 1.489 emu/g = $Ce_{0.7}Tb_{0.3}O_2$	97
La-doped	calcination	3.21 = undoped; 3.08 = La-doped	undoped ceria = spherical; La-doped= grain like	magnetic	magnetization values: 0.9 × 10^{-3} emu/g = undoped ceria; 19.6 × 10^{-3} emu/g = 8% La-doped	98
Pr-doped	microwave-assisted	0.04 doped = 2.65; 0.08 doped = 2.69; 0.12 doped = 2.88	Pr-doped showed agglomerates	magnetic	all are superparamagnetic below T_B	99

https://doi.org/10.1021/acsomega.3c01199
ACS Omega XXXX, XXX, XXX−XXX

Table 5. Synthesis, Properties, and Applications of Dual Metal Doped Ceria

material	synthesis method	band gap energy (eV)	morphology	application	findings	ref
Sb- and Bi-doped	co-precipitation	not reported	agglomerated sheets	conductivity	conductivity values (S cm^{-1}): 2.66×10^{-3} = $Ce_{0.8}Sm_{0.2}O_{2-\delta}$ 3.77×10^{-5} = $Ce_{0.8}Sm_{0.1}Sb_{0.1}O_{2-\delta}$ 3.18×10^{-3} = $Ce_{0.8}Sm_{0.1}Bi_{0.1}O_{2-\delta}$	100
Mn/Fe-, Cu/Ag-, Fe/Cu-, and Mn/Cu-doped	hydrothermal	2.98 = Mn/Fe-doped; 3.09 = Cu/Ag-doped; 2.35 = Fe/Cu-doped; 2.26 = Mn/Cu-doped	not reported	reduction of exhaust emission	Mn/Cu-doped ceria showed the best catalytic activity	48
Sn/Zr-doped	green	2.66 = undoped ceria; 2.58 = 1% Sn/Zr-doped; 2.49 = 5% Sn/Zr-doped; 2.54 = 10% Sn/Zr-doped	spherical NPs of size 12−17 nm	photoantioxidant and biofilm activities	10% Zr/Sn responded to inhibiting biofilm formation and antibacterial activities	15
Sm/Nd-doped	sintering	not reported	average grain size between 3 and 6 μm	electromechanical	electrorestrictive coefficient above 10^{-17} $(m/V)^2$ at a low frequency	101

an emphasis on producing controllable morphologies and tunable band gap energies that can be applied in numerous biomedical and catalytic applications.

3.2. Non-metal Doped Ceria. Ceria NPs have been doped with non-metals such as nitrogen (N), sulfur (S), and phosphorus (P). These non-metals increase the light-harvesting or absorption ability of ceria in the visible region, which can be explained by the hybridization that takes place between the p orbitals of the non-metal and the oxygen atoms in ceria, leading to an upward movement of the VB edge, as illustrated in Figure 6, thus leading to a reduction in the band gap.

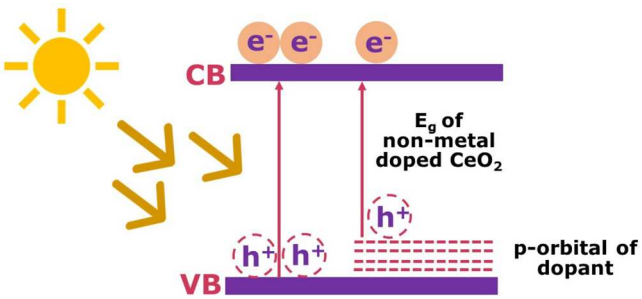

Figure 6. Creation of band gap states and modification of the band gap energy in non-metal doped ceria.

3.2.1. Nitrogen-Doped Ceria. N-doped ceria NPs have been synthesized with different methods, and their properties investigated. N-doped ceria was synthesized using a deep eutectic solvent in an autoclave and was investigated for photocatalytic sulfamethoxazole (SMX) degradation.[11] The N-doped ceria removed 96% of SMX, significantly more than undoped ceria, which had an efficiency of only 59%. The irradiation of the photocatalysts generated hydroxyl radicals, $^{\bullet}OH$, which in turn reacted with SMX and caused it to degrade. Thus, the reduced energy band gap of N-doped ceria (2.72 eV) facilitates its activity by generating more $^{\bullet}OH$ compared to the undoped ceria (3.03 eV). In other work, N-doped ceria was prepared by heat treatment with urea as a nitrogen source, and by controlling the temperature and mass ratio of ceria/urea, interstitial or substitutional site doping was achieved.[102] Nitrogen introduced at both interstitial and substitutional sites was tested for the removal of SMX, and the results revealed that N incorporated at interstitial sites in the ceria led to more oxygen vacancies and showed better performance with an efficiency of 94% within 30 min, while only 72% was obtained for N introduced into substitutional sites.

Furthermore, Shen and co-workers also synthesized N-doped ceria by a urea-assisted template method. TEM observations revealed a mesoporous morphology for the N-doped ceria, with a pore size of ∼3.75 nm and a less regular structure compared with undoped ceria with pore size of about 3.49 nm.[14] The N-doped ceria has a reduced band gap energy (2.45 eV) and displayed better CO_2 adsorption and a higher oxygen vacancy concentration compared with undoped ceria. Hence, N-doped ceria showed a higher efficiency for the photocatalytic conversion of CO_2 to CO and CH_4, with yields of 1.83 and 1.25 μmol/g, respectively, while the undoped ceria produced 0.73 and 0.42 μmol/g of CO and CH_4, respectively.

Dual-doped or co-doped ceria with non-metal dopants has also been investigated as it has advantages of producing more oxygen vacancies, enhancing charge separation, and possessing

https://doi.org/10.1021/acsomega.3c01199
ACS Omega XXXX, XXX, XXX−XXX

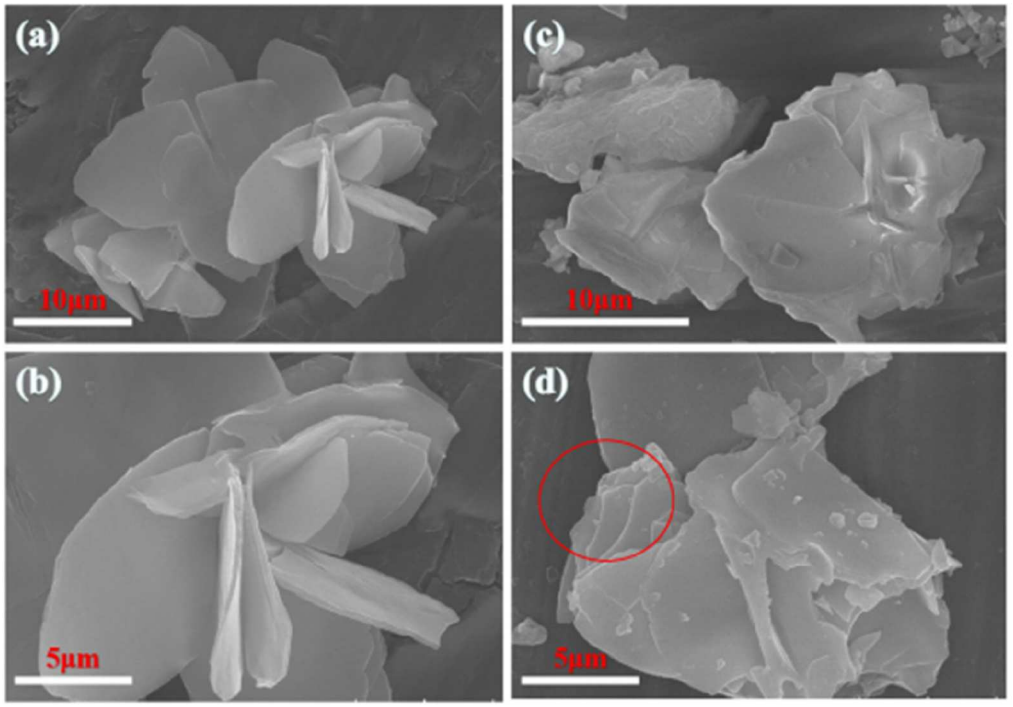

Figure 7. SEM images illustrating the lamellar structure of undoped (a, b) and P-doped ceria (c, d). Reproduced from ref 106 with permission from Elsevier, Copyright 2020.

superior light harvesting efficiency. Masingh and co-workers synthesized S/N co-doped ceria nanostructures by the hydrothermal method at different reaction times of 24, 36, and 48 h.[103] The obtained materials were tested for the photoreduction of Cr^{6+}. The band gap energies obtained were 2.94, 2.45, 2.24, and 2.17 eV for the undoped and doped ceria at 24, 36, and 48 h, respectively. The photoreduction tests carried out revealed that the doped ceria prepared at 36 h displayed the best performance with 93% reduction, while only 19% was obtained for the undoped ceria. The better performance exhibited by the doped ceria prepared at 36 h was evident in its high photocurrent density (3.87 mA/cm^2) and longer decay time of about 76 ps, all these facilitate a higher concentration of excited electrons and more visible light absorption capacity. Similarly, N/S co-doped ceria was prepared by calcination treatment, and its photocatalytic properties were investigated.[104] The photocurrent response studied over time showed that the current intensity of the N/S-doped ceria was higher (275 $\mu A/cm^2$) compared with those of the undoped ceria (115 $\mu A/cm^2$) and the commercial ceria (102 $\mu A/cm^2$). The photoluminescence also revealed that the intensity of the doped ceria decreased and shifted to a more visible region indicating lower band gap energy and better light response. The photocatalytic degradation of acetaldehyde to CO_2 investigated for the doped ceria and commercial ceria indicated that the CO_2 produced with the doped ceria was greater (1092 ppm) than that of commercial ceria (150 ppm). N/P dual-doped ceria/carbon was synthesized by the calcination method and tested as a catalyst for the degradation of ciprofloxacin.[105] The undoped ceria showed only 62% efficiency at 3 h, while N-doped ceria recorded 79%, and the highest value was obtained with the dual-doped ceria showing a 95% degradation efficiency. The increased efficiency of the dual-doped ceria was due to the availability of higher oxygen vacancies and more carbon content, resulting in the improved electron transport ability needed for the degradation process. The morphology of the undoped ceria particles is that of a uniform sphere, while the doped ceria particles have irregular shapes.

3.2.2. Phosphorus-Doped Ceria. Phosphorus (P)-doped ceria was synthesized by a bio-based calcination method, and its effect on the thermal and fire safety of epoxy resin (ER) was investigated. The results revealed that the ER has improved thermal and fire stability with the introduction of P.[106] The above observation was explained by the increased thermal degradation temperature when P-doped ceria was introduced into ER, and it is also evident in other parameters such as decreased CO production, total smoke production, and peak heat release rate. The better fire safety performance was evaluated using fire growth index value; this value decreases from 9.46 kW/m^2 s (ER) to 8.96 kW/m^2 s for ceria/ER, and the lowest value of 8.46 kW/m^2 s was recorded for P-doped ceria/ER. SEM observations revealed that both undoped and P-doped ceria adopted lamellar structures with smooth surfaces (Figure 7). In another study, P-doped ceria/titania nanocomposite was synthesized by a solution combustion method.[107] SEM showed that the sample is porous, and the band gap energy of the P-doped ceria/titania increases with increasing temperature; 2.93, 2.90, and 2.89 eV were obtained at 400, 500, and 600 °C respectively.

Furthermore, P-doped ceria was synthesized by a calcination method, and SEM images revealed the formation of nanorods.[108] The capacitance recorded in a lithium sulfide battery showed a high initial capacity of 1027 mA h/g compared to undoped ceria, which achieved only 896 mA h/g. The P-doped ceria cathode also exhibited a modest capacity decay of only ~0.1% per cycle after 500 cycles at 1 C.

3.2.3. Halogen Doped Ceria. F-doped ceria was prepared by the co-precipitation method and tested as a catalyst in the oxidation of toluene.[109] It was found that the conversion

https://doi.org/10.1021/acsomega.3c01199
ACS Omega XXXX, XXX, XXX−XXX

Table 6. Synthesis, Properties, and Applications of Non-metal Doped Ceria

material	synthesis method	band gap energy (eV)	morphology	application	performance	ref
N-doped	deep eutectic solvent in autoclave	2.72 = N-doped ceria; 3.03 = undoped ceria	N-doped showed platelets, average size = 12 nm	photocatalytic degradation of SMX	N-doped ceria = 96% removal; undoped ceria = 59% removal	11
N-doped	urea-assisted template method	2.45 = N-doped ceria	N-doped showed a mesoporous structure	photocatalytic conversion of CO_2	yield of CO and CH_4, respectively: 1.83 and 1.25 μmol/g = N doped; 0.73 and 0.42 μmol/g = undoped ceria	14
N-doped	heat treatment	not reported	nanorod diameter = 4−12 nm, length = 40−150 nm	photocatalytic degradation of SMX	N on interstitial site = 94% removal; N on substitutional site = 72% removal	102
S/N co-doped	hydrothermal	2.94 = undoped; 2.45 = 24 h; 2.24 = 36 h; 2.17= 48 h	dual-doped showed average size of 8 nm	photoreduction of Cr^{6+}	sample at 36 h = 93% reduction; undoped ceria = 19% reduction	103
S/N co-doped	calcination	N/S co-doped = 2.98	dual-doped showed nanorods	photocatalytic degradation of acetaldehyde	CO_2 produced: 1092 ppm = doped ceria; 150 ppm = undoped ceria	104
P-doped ceria/ER	biocalcination	not reported	lamellar structure	fire and thermal stability of ER	fire growth index value: 9.46 kW/m^2 s = ER; 8.96 kW/m^2 s = ceria/ER; 8.46 kW/m^2 s = P-doped ceria/ER	106
N/P-dual-doped ceria/C	calcination	not reported	sphere = undoped ceria; irregular shape = doped	degradation of ciprofloxacin	efficiency: 62% = undoped; 79% = N-doped; 95% = N/P dual-doped	105
P-doped ceria/titania	solution combustion	0.93 = 400 °C; 2.90 = 500 °C; 2.89 = 600 °C	porous structure	optical	enhanced absorption with increasing temperature	107
P-doped	calcination	not reported	P-doped= nanorod of size 10 nm	cathode in LiS battery	initial capacitance value: 1027 mA h/g = P-doped; 896 mA h/g = undoped ceria	108
F-doped	co-precipitation	not reported	mesoporous structure	oxidation of toluene	conversion temperature (50 and 90%): 218 and 306 °C = F-doped; 233 and 336 °C = undoped ceria	109
Cl-doped ceria/CNT	calcination	not reported	undefined	cathode in LiS battery	initial discharge capacity: 821 mAh/g = Cl-doped; 688 mAh/g= undoped ceria	110
S-doped ceria/CNT	hydrothermal	2.24 = S-doped; 2.84 = undoped ceria	undefined	cathode in LiS battery	discharge capacity = 1380 mAh/g; 90% retention after 500 cycles	111
S-doped	solid state	2.84 = S-doped; 3.7 = undoped ceria	S-doped= egg-shaped mesoporous; undoped ceria= cubic shaped	photocatalytic degradation of methyl orange	degradation efficiency: 98.6% = S-doped; 42.2% = undoped ceria	112

https://doi.org/10.1021/acsomega.3c01199
ACS Omega XXXX, XXX, XXX−XXX

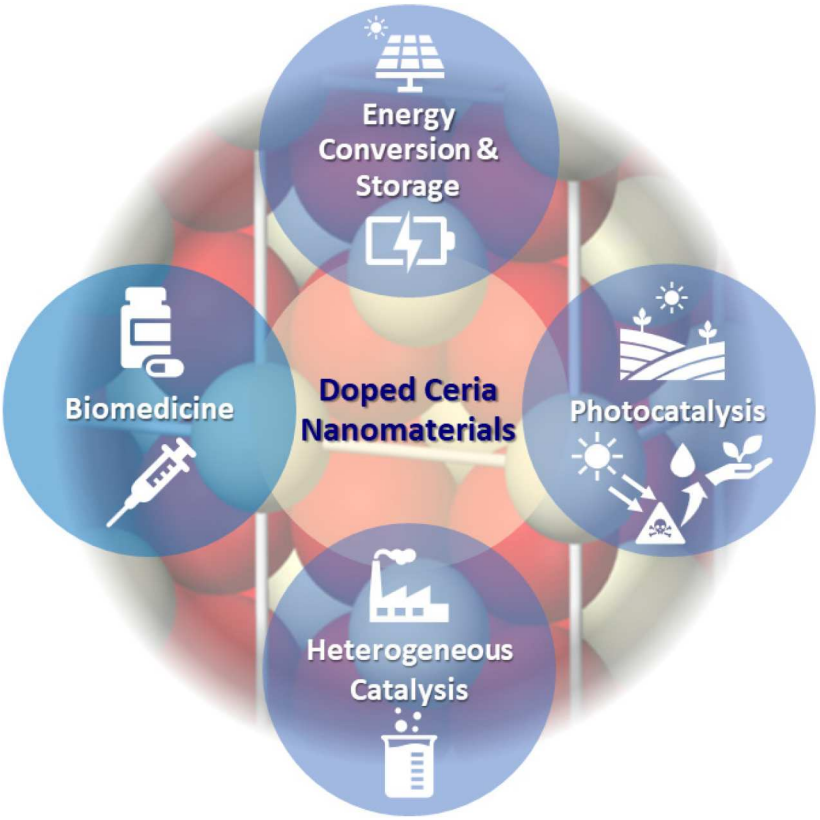

Figure 8. Various applications of doped ceria nanomaterials.

temperature of the optimal F-doped ceria (F/Ce = 0.03) is 218 and 306 °C at 50% and 90%, respectively, while the undoped ceria recorded 233 and 336 °C. This is due to the fact that the F-doped ceria has more oxygen vacancies as revealed by its XPS analysis. Furthermore, Cl-doped ceria/CNT was synthesized by the calcination method and tested as an electrode in a lithium−sulfur battery.[110] It was found that the Cl-doped ceria had the highest initial discharge capacity of 820.8 mAh/g, while the undoped ceria/CNT recorded a value of 687.6 mAh/g. Moreover, the capacity retention of Cl-doped ceria/CNT was 83% even after 200 cycles.

3.2.4. Sulfur-Doped Ceria. Sulfur-doped ceria/CNT prepared by the hydrothermal method was tested as a cathode material in lithium−sulfur battery.[111] The result showed that the S-doped ceria has a high discharge capacity of 1380 mAh/g with 90% retention even after 500 cycles. The good performance of the S-doped ceria was explained by the fact that it has a lower band gap energy of 2.24 eV compared with undoped ceria (2.84 eV) which favors the migration of electrons and its adsorption capacity.

In other work, S-doped ceria prepared by the solid-state method using sodium benzenesulfonate as a template was tested for the photocatalytic degradation of methylene orange.[112] The SEM revealed an egg-shaped morphology of mesoporous material, and the inclusion of S led to the narrowing of band gap with a value of 2.84 eV recorded for the S-doped ceria, while the undoped ceria gave 3.7 eV. The degradation efficiency showed that the S-doped ceria gave the best performance (98.6%) compared with the undoped ceria with only a 42.2% efficiency which has been attributed to the higher surface area of the S-doped ceria as evident in the BET.

Table 6 summarizes the preparation routes, properties, and applications of non-metal doped ceria.

Non-metal doped ceria has mostly been synthesized by calcination or solid-state synthesis methods with relatively few reports of wet chemical methods compared with metal doped ceria. This in turn will affect the morphology and properties of the prepared powders and ultimately the performance of the material in a given application. There does not appear to be any fundamental reason that solid-state synthesis methods should be preferred, and indeed, a few reports of hydrothermal and co-precipitation synthesis of non-metal doped ceria are promising. Calcination and other solid-stage synthesis methods clearly have some disadvantages in that sintering of particles during the heat treatment tends to result in lower specific surface area and consequently lower catalytic activity. It is therefore necessary to further explore other preparation routes, particularly wet chemical routes, in order to expand the utility of non-metal doped ceria nanomaterials.

4. APPLICATIONS OF DOPED CERIA

Doped ceria nanomaterials have proven useful for applications encompassing photocatalysis, biomedicine, and energy conversion and storage, among others, as illustrated in Figure 8. Such broad utility is a testament to the range of novel properties that can be accessed by judicious doping of ceria nanomaterials with metals or non-metals.

4.1. Photocatalysis. In photocatalysis, a major factor that contributes to the improved performance of doped ceria is the reduction in the band gap energy and consequent hindrance of the recombination process. Also of importance is the creation of Ce^{3+} and the generation of oxygen vacancies.[113] Doped ceria NPs have been employed in the cleanup of the environment by

https://doi.org/10.1021/acsomega.3c01199
ACS Omega XXXX, XXX, XXX−XXX

the photocatalytic degradation of pharmaceutical and chemical pollutants. For instance, Iqbal and co-workers used N-doped ceria for the photocatalytic degradation of sulfamethoxazole.[11] The N-doped ceria gave an efficiency of 96%, while the undoped ceria has only 59% efficiency. Furthermore, N/P dual-doped ceria/carbon has also been used for the degradation of ciprofloxacin.[105] The undoped ceria exhibited only 62% efficiency, followed by 79% for N-doped ceria, while the highest degradation efficiency of 95% was recorded for the dual-doped ceria.

The removal of chemical pollutants like acetaldehyde and Cr^{6+} has been achieved by the use of N/S dual-doped ceria[103,104] In addition, metal doped ceria nanomaterials have been tested as photocatalysts. The photocatalytic degradation of rhodamine B was investigated using Mn-, Fe-, La-, and Pr-doped ceria.[63] The photoluminescence spectra revealed that there is a red shift with doped ceria, and the highest shift was recorded for the Mn-doped ceria. Hence, Mn^{3+}-doped ceria showed the best photocatalytic response followed by Fe^{3+}-doped ceria, while the La^{3+}- and Pr^{3+}-doped ceria showed a reduced response. Furthermore, photocatalytic degradation activities of Ag-, Au-, and Pt-doped ceria have been evaluated, and it was found that Au-doped ceria is the most active having a degradation efficiency greater than 98%.[79]

Non-metal doped ceria has been applied in the photocatalytic conversion of CO_2 to produce fuels using N-doped ceria. The production of CO and CH_4 with yields of 1.83 and 1.25 μmol/g, respectively, was obtained with N-doped ceria while the undoped ceria produced 0.73 and 0.42 μmol/g of CO and CH_4, respectively. In addition, the photocatalytic conversion of CO_2 was investigated using Mo-, Y-, and La-doped ceria.[12] The Y-doped ceria displayed the best performance generating 22 ppm of CO gas followed by Mo-doped ceria generating 8 ppm of CO.

4.2. Biomedicine. Doped ceria NPs have also been applied in the field of biomedicine as antibacterial, antioxidant, and anticancer agents. The suitability of doped ceria for these applications is mainly due to the increased presence of oxygen vacancies in the ceria crystal lattice, which can act as electron donors or acceptors and thus enable the participation of doped ceria in various redox reactions. For instance, Sisubalan and co-workers synthesized Mg-, Ca-, Sr-, and Ba-doped ceria and found that Ba-doped ceria had the highest biocidal activity, which was attributed to the small particle size, leading to easy penetration into the bacterial cell membrane. Interestingly, cytotoxicity tests carried out using fibroblast cells revealed that Ba-doped ceria was less toxic to healthy cells.[45] In related work, Naidi and co-workers prepared Zr-doped ceria using a green method, and the tests carried out showed better antioxidant properties under visible light irradiation compared to the dark in a concentration-dependent manner.[51] Optimum biocidal properties were obtained at 512 μg/mL for 1% Zr-doped ceria, while the undoped ceria required 1024 μg/mL, and reduced activities were observed for 5% and 10% Zr-doped ceria. Biofilm inhibition studies showed 73% inhibition of *S. aureus* at 512 μg/mL for the undoped ceria, while the 10% Zr-doped ceria inhibited film formation by 53%. A similar result was obtained by the same author using Sn-doped ceria; the activity of the doped ceria was concentration dependent, and greater biocidal effects were obtained at higher concentrations of Sn (10%).

Aside from single dopant doped ceria, dual Sn/Zr-doped ceria has also been investigated for antibacterial and antioxidant properties by Naidi and co-workers.[15] The results showed that at a higher concentration only the 10% Zr/Sn dual-doped ceria and undoped ceria NPs were effective in killing the bacteria. Irrespective of the concentration used, enhanced antioxidant activities were observed in visible light compared to the dark. The cytotoxicity of Ag-doped ceria toward EPG human gastric cancer cells was investigated, and the results showed that activity was concentration dependent, with no significant cytotoxic effects up to 62.5 mM.[78] The anticancer activity of Fe-doped ceria has also been studied, and it was found that the activity is dependent on both the concentration of Fe-doped ceria and the time of incubation.[72] Half maximal inhibitory concentrations (IC_{50}) of 6.1 and 3.02 mg/mL were recorded for the Fe-doped ceria NPs after 48 and 72 h exposure, respectively. Saravanakumar and co-workers investigated the cytotoxicity of PEGylated Pd-doped ceria and compared it with Pd NPs and ordinary Pd-doped ceria.[81] These were tested on a human lung cancer cell line, and the findings revealed that the PEGylated Pd-doped ceria exhibited strong cytotoxicity with $IC_{50} \sim 81.25$ μg/mL, followed by Pd-doped ceria (~118.75 μg/mL), and last, ~231.25 μg/mL was obtained for Pd NPs.

4.3. Energy Conversion and Storage. The application of doped ceria in energy storage and conversion processes, including batteries, the water−gas shift reaction (WGS), fuel cells, and supercapacitors, has been reported. Non-metal doped ceria (N, P, and Cl) has been used as a cathode material in lithium sulfur batteries with remarkable performance. For instance, P-doped ceria in a lithium sulfide battery showed a high initial capacity of 1027 mA h/g compared to undoped ceria, which gave a value of 896 mA h/g.[108] Furthermore, the P-doped ceria cathode exhibited a low decay in capacity (~0.10% per cycle after 500 cycles at 1.0 C). In addition, the use of Cl-doped ceria in a lithium battery was investigated by Fan and co-workers, and the results revealed that the Cl-doped ceria had better performance with the highest initial discharge capacity of 820.8 mAh/g, while the undoped ceria/CNT recorded a value of 687.6 mAh/g.[110] S-doped ceria has also been tested as a cathode material in lithium batteries, and the results revealed that the S-doped ceria has a high discharge capacity of 1380 mAh/g with 90% capacity retention even after 500 cycles.[111] This performance was attributed to the lower band gap energy of S-doped ceria (2.24 eV) compared with undoped ceria (2.84 eV).

In research conducted by Ang and co-workers,[53] Na-doped ceria NPs were used in the WGS reaction to improve the production of CO_2 by suppressing the unwanted methanation reaction. The results showed that the performance improvement was concentration dependent, with the highest yield of 97.5% being achieved for CO_2 generated with 2 wt % Na doping, but upon increasing the doping to 5 and 10 wt %, the yield decreased to 97.1% and 94.4%, respectively. A comparison between two methods of preparation (co-precipitation and mechanochemical activation) and the resulting WGS activity was carried out by Tabakova and co-workers.[62] Their findings revealed that the samples prepared by mechanochemical activation had better catalytic activity than those prepared using co-precipitation, with Fe- and Mn-doped ceria displaying the best performance over the Sn-doped ceria. The better performance was attributed to the fact that the doped samples prepared by the mechanochemical conversion had a greater proportion of smaller sized particles compared with those prepared by the co-precipitation route.

https://doi.org/10.1021/acsomega.3c01199
ACS Omega XXXX, XXX, XXX−XXX

The use of V-doped ceria as a catalyst to improve syngas production has also been reported.[75] The results revealed that the syngas production increased using V-doped ceria with a corresponding decrease in the activation temperature; 784 °C was recorded for V-doped ceria, while the undoped ceria required 962 °C. The application of Fe-doped ceria in pseudocapacitors has been investigated by Lee and co-workers who found that Fe-doped ceria exhibited excellent cycling stability and a high specific capacitance of 559 F/g, while the undoped ceria gave ∼121 F/g at 1 A/g.[71] Mn-, Fe-, Co-, Ni-, and Cu-doped ceria have also been tested as catalysts in fuel cells.[59] The photoreduction of CO_2 by Y-, La-, and Mo-doped ceria was carried out by Wang and co-workers, and the results revealed that the Y-doped ceria had the best performance producing 22 ppm of CO gas in the first hour, followed by Mo-doped ceria with 8 ppm of CO generated in the first 3 h.[12]

4.4. Heterogeneous Catalysis. Doped ceria NPs have also been employed as catalysts in various reactions. For instance, Cu-doped ceria prepared by the thermolysis of a MOF precursor has been used for the oxidation of CO.[64] The nanostructures were obtained from two different ligands, benzene dicarboxylic acid (BDC) and 4,4-biphenyl dicarboxylic acid (BPDC), and the catalytic results revealed that, for the conversion of CO into CO_2, the conversion temperatures of the two Cu-doped ceria nanostructures are 110 and 140 °C for BPDC and BDC, respectively. The better catalytic activity of Cu-doped ceria from BPDC is in line with its higher surface area. Similarly, Sm-doped ceria was also tested as a catalyst in the oxidation of CO, and the findings showed the Sm-doped ceria has a better performance because of its higher surface area with at least a 70% conversion while the undoped ceria barely has 40% conversion.[87]

Doped ceria has also been investigated as a catalyst in organic reactions. For instance, Cu-, Ni-, Fe-, Co-, and Mn-doped ceria have been tested for the oxidation of toluene, and their efficiency was evaluated by taking the temperature at which 50% of the toluene was converted.[60] The results obtained were 267, 217, 231, 242, and 254 °C for undoped and Cu-, Mn-, Zn-, and Fe-doped ceria, respectively. In addition, non-metal (F) doped ceria was also tested in the oxidation of toluene, and it was found that the 50% conversion temperature of the F-doped ceria was 218 °C, while that of undoped ceria was 233 °C. This is due to the fact that the F-doped ceria has more oxygen vacancies, as revealed by its XPS analysis.[109] The s block doped ceria has been used in the dehydration of alcohol. For instance, Na-doped ceria was investigated as a catalyst for the dehydration of 1,5-pentanediol.[54] The results revealed that the doped ceria was more selective than the undoped ceria, thus suppressing unwanted side reactions. Furthermore, Ca-doped ceria has been tested for the dehydration of 2-octanol.[55] The results revealed that 0.15 wt % Ca-doped ceria, which has the smallest size, displayed the best performance, while the efficiency of the undoped ceria dropped after some time. The performance of Gd-doped ceria in soot oxidation was evaluated using two different methods of preparation: the solvothermal and citrate methods.[90] The findings revealed that the Gd-doped ceria prepared from the citrate method had a lower band gap energy and more surface oxygen, leading to better performance with a lower T_{50} value of 468 °C, while the ceria produced using the solvothermal method had a higher T_{50} value of 500 °C.

5. FUTURE OUTLOOK

Although steady progress in the synthesis of doped ceria nanomaterials has been achieved for various applications, there are still insufficient data in certain areas that require attention. In particular, the following general issues need to be addressed to optimize the preparation of doped ceria and fully understand its role in specific applications:

- Further research into reaction mechanisms, including theoretical calculations and simulations, is required to optimize the catalytic reactivity and stability of doped ceria and to establish the optimal weight percentages of the dopant.
- The relationships between factors such as the ionic radii of dopants, their redox potential, how they affect the oxygen vacancy concentration, and their eventual performance in applications must be established.
- More systematic research is required to disentangle the effects of different types of dopants on the intrinsic material properties of doped ceria (e.g., band gap, absorption coefficient, carrier mobilities) versus simple changes in particle morphology and surface area. Such information would be invaluable when designing synthesis routes to produce the desired overall properties in catalytic and photocatalytic applications.
- There is a need to explore the green synthesis of s block metal doped ceria and to extend its applications to biological fields.
- Both metal and non-metal doped ceria should be explored for solar energy applications, such as the photocatalytic reduction of CO_2 and photoelectrochemical water splitting.
- Alternative methods of synthesis for non-metal doped ceria should be explored to obtain novel properties and broaden the range of applications of ceria nanomaterials.

6. CONCLUSION

Doped ceria nanomaterials have potential applications not only in conventional catalysis but also in fields as diverse as photocatalysis and biomedicine. Ceria nanoparticles are generally amenable to doping with both metal and non-metal dopants, and judicious selection of the dopant, as well as control of the dopant and oxygen vacancy concentrations, can enhance the performance of ceria nanomaterials in their many applications. This review provided a concise overview of the dopants that have been successfully incorporated into the ceria crystal lattice, including s block, p block, d block, and f block metals and metalloids, as well as non-metals such as N, S, and P. Where applicable, the synthetic methods used to prepare doped ceria were highlighted, and the effects of doping on the catalytic, photocatalytic, antibacterial, and energy applications of ceria were discussed. A common theme across all dopants and applications was that the concentration of dopant in the ceria lattice was a key factor in determining the performance of the material. In general, metal dopants tend to create new states near the conduction band edge and lower the energy of the conduction band, while non-metal dopants tend to raise the valence band edge. These changes in electronic structure cause a desirable narrowing of the band gap and more active surface states, which are beneficial in most applications of doped ceria nanomaterials. Finally, this review highlights the remaining issues that need to be addressed to further optimize

https://doi.org/10.1021/acsomega.3c01199
ACS Omega XXXX, XXX, XXX−XXX

the synthesis of doped ceria nanomaterials to obtain desirable properties for existing and new applications.

AUTHOR INFORMATION

Corresponding Authors

Mohammad Mansoob Khan − *Chemical Sciences, Faculty of Science, Universiti Brunei Darussalam, Gadong BE 1410, Brunei Darussalam; Optoelectronic Device Research Group, Universiti Brunei Darussalam, Gadong BE 1410, Brunei Darussalam;* orcid.org/0000-0002-8633-7493; Email: mansoob.khan@ubd.edu.bn

James Robert Jennings − *Applied Physics, Faculty of Science, Universiti Brunei Darussalam, Gadong BE 1410, Brunei Darussalam; Optoelectronic Device Research Group, Universiti Brunei Darussalam, Gadong BE 1410, Brunei Darussalam;* orcid.org/0000-0002-8887-4794; Email: james.jennings@ubd.edu.bn

Author

Khadijat Olabisi Abdulwahab − *Applied Physics, Faculty of Science, Universiti Brunei Darussalam, Gadong BE 1410, Brunei Darussalam; Department of Chemistry, Faculty of Science, University of Lagos, Lagos 101017, Nigeria*

Complete contact information is available at: https://pubs.acs.org/10.1021/acsomega.3c01199

Notes

The authors declare no competing financial interest.

ACKNOWLEDGMENTS

This research was funded by Universiti Brunei Darussalam through grants UBD/RSCH/1.4/FICBF(b)/2022/046 and UBD/RSCH/URC/NIG/8.0/2021/001. Khadijat Olabisi Abdulwahab wishes to express appreciation to the Islamic Development Bank (IDB) for the award of a postdoctoral scholarship (award number SCHD-277).

REFERENCES

(1) Montini, T.; Melchionna, M.; Monai, M.; Fornasiero, P. Fundamentals and Catalytic Applications of CeO2-Based Materials. *Chem. Rev.* **2016**, *116* (10), 5987−6041.

(2) Mogensen, M.; Sammes, N. M.; Tompsett, G. A. Physical, Chemical and Electrochemical Properties of Pure and Doped Ceria. *Solid State Ionics* **2000**, *129* (1), 63−94.

(3) Naidi, S. N.; Khan, F.; Tan, A. L.; Harunsani, M. H.; Kim, Y. M.; Khan, M. M. Photoantioxidant and Antibiofilm Studies of Green Synthesized Sn-Doped CeO2nanoparticles Using Aqueous Leaf Extracts of: Pometia Pinnata. *New J. Chem.* **2021**, *45* (17), 7816−7829.

(4) Zhang, D.; Du, X.; Shi, L.; Gao, R. Shape-Controlled Synthesis and Catalytic Application of Ceria Nanomaterials. *Dalt. Trans.* **2012**, *41* (48), 14455−14475.

(5) Parwaiz, S.; Bhunia, K.; Das, A. K.; Khan, M. M.; Pradhan, D. Cobalt-Doped Ceria/Reduced Graphene Oxide Nanocomposite as an Efficient Oxygen Reduction Reaction Catalyst and Supercapacitor Material. *J. Phys. Chem. C* **2017**, *121* (37), 20165−20176.

(6) Yang, W.; Wang, X.; Song, S.; Zhang, H. Syntheses and Applications of Noble-Metal-Free CeO2-Based Mixed-Oxide Nanocatalysts. *Chem* **2019**, *5*, 1743−1774.

(7) Naidi, S. N.; Harunsani, M. H.; Tan, A. L.; Khan, M. M. Green-Synthesized CeO2nanoparticles for Photocatalytic, Antimicrobial, Antioxidant and Cytotoxicity Activities. *J. Mater. Chem. B* **2021**, *9* (28), 5599−5620.

(8) Naidi, S. N.; Harunsani, M. H.; Tan, A. L.; Khan, M. M. Structural, Morphological and Optical Studies of CeO2 Nanoparticles Synthesized Using Aqueous Leaf Extract of Pometia Pinnata. *Bionanoscience* **2022**, *12* (2), 393−404.

(9) Alowakennu, M.; Adams, L. A.; Abdulwahab, K. O. Synthesis of Ceria (CeO 2) Nanoparticles and Their Application in Colorimetric Probes for the Determination of Ascorbic Acid. *ChemistrySelect* **2022**, *7*, 202103463.

(10) Mužina, K.; Kurajica, S.; Dražić, G.; Guggenberger, P.; Matijašić, G. True Doping Levels in Hydrothermally Derived Copper-Doped Ceria. *J. Nanoparticle Res.* **2021**, *23* (7), 1−14.

(11) Iqbal, J.; Shah, N. S.; Sayed, M.; Ali Khan, J.; Muhammad, N.; Khan, Z. U. H.; Saif-ur-Rehman; Naseem, M.; Howari, F. M.; Nazzal, Y.; Niazi, N. K.; Hussein, A.; Polychronopoulou, K. Synthesis of Nitrogen-Doped Ceria Nanoparticles in Deep Eutectic Solvent for the Degradation of Sulfamethaxazole under Solar Irradiation and Additional Antibacterial Activities. *Chem. Eng. J.* **2020**, *394*, 124869.

(12) Wang, M.; Shen, M.; Jin, X.; Tian, J.; Shao, Y.; Zhang, L.; Li, Y.; Shi, J. Exploring the Enhancement Effects of Hetero-Metal Doping in CeO2 on CO2 Photocatalytic Reduction Performance. *Chem. Eng. J.* **2022**, *427*, 130987.

(13) Kundu, S.; Sutradhar, N.; Thangamuthu, R.; Subramanian, B.; Panda, A. B.; Jayachandran, M. Fabrication of Catalytically Active Nanocrystalline Samarium (Sm)-Doped Cerium Oxide (CeO2) Thin Films Using Electron Beam Evaporation. *J. Nanoparticle Res.* **2012**, *14*, 1040.

(14) Shen, Z.; Xia, Q.; Li, Y.; Yin, C.; Ge, Z.; Li, X.; Wang, Y. Adsorption-Enhanced Nitrogen-Doped Mesoporous CeO2as an Efficient Visible-Light-Driven Catalyst for CO2photoreduction. *J. CO2 Util.* **2020**, *39*, 101176.

(15) Naidi, S. N.; Khan, F.; Tan, A. L.; Harunsani, M. H.; Kim, Y. M.; Khan, M. M. Green Synthesis of Ceo2and Zr/Sn-Dual Doped Ceo2nanoparticles with Photoantioxidant and Antibiofilm Activities. *Biomater. Sci.* **2021**, *9* (14), 4854−4869.

(16) Mishra, S. R.; Ahmaruzzaman, M. Cerium Oxide and Its Nanocomposites: Structure, Synthesis, and Wastewater Treatment Applications. *Mater. Today Commun.* **2021**, *28* (March), 102562.

(17) Shehata, N.; Samir, E.; Gaballah, S. New Optical Sensor for Peroxides Using Neodymium-Doped-Ceria Nanoparticles via Fluorescence-Quenching Technique. *Sensors Actuators, B Chem.* **2016**, *231*, 341−348.

(18) Zhou, M.; Church, A. L.; Cordon, M. J.; Li, C.; Hunt, R. D.; Choi, J.; Bai, L.; Li, Z.; Parks, J. E.; Hu, M. Z.; Curtiss, L. A.; Assary, R. S. Mechanistic Insights and Rational Design of Ca-Doped CeO2 Catalyst for Acetic Acid Ketonization. *ACS Sustain. Chem. Eng.* **2022**, *10* (34), 11068−11077.

(19) Wang, X.; Li, M.; Wu, Z. In Situ Spectroscopic Insights into the Redox and Acid-Base Properties of Ceria Catalysts. *Chin. J. Catal.* **2021**, *42* (12), 2122−2140.

(20) Tran, D. P. H.; Pham, M. T.; Bui, X. T.; Wang, Y. F.; You, S. J. CeO2 as a Photocatalytic Material for CO2 Conversion: A Review. *Sol. Energy* **2022**, *240* (April), 443−466.

(21) Zhou, J.; Guo, R. T.; Zhang, X. F.; Liu, Y. Z.; Duan, C. P.; Wu, G. L.; Pan, W. G. Cerium Oxide-Based Catalysts for Low-Temperature Selective Catalytic Reduction of NOxwith NH3: A Review. *Energy Fuels* **2021**, *35* (4), 2981−2998.

(22) Du, Y.; Gao, F.; Zhou, Y.; Yi, H.; Tang, X.; Qi, Z. Recent Advance of CuO-CeO2 Catalysts for Catalytic Elimination of CO and NO. *J. Environ. Chem. Eng.* **2021**, *9* (6), 106372.

(23) Jaiswal, N.; Tanwar, K.; Suman, R.; Kumar, D.; Upadhyay, S.; Parkash, O. A Brief Review on Ceria Based Solid Electrolytes for Solid Oxide Fuel Cells. *J. Alloys Compd.* **2019**, *781*, 984−1005.

(24) Xie, S.; Wang, Z.; Cheng, F.; Zhang, P.; Mai, W.; Tong, Y. Ceria and Ceria-Based Nanostructured Materials for Photoenergy Applications. *Nano Energy* **2017**, *34*, 313−337.

(25) Lu, G.; Zheng, H.; Lv, J.; Wang, G.; Huang, X. Review of Recent Research Work on CeO2-Based Electrocatalysts in Liquid-Phase Electrolytes. *J. Power Sources* **2020**, *480*, 229091.

(26) Kurian, M. Journal of Environmental Chemical Engineering Cerium Oxide Based Materials for Water Treatment - A Review. *J. Environ. Chem. Eng.* **2020**, *8* (5), 104439.

(27) Shan, Y.; Liu, Y.; Li, Y.; Yang, W. A Review on Application of Cerium-Based Oxides in Gaseous Pollutant Purification. *Sep. Purif. Technol.* **2020**, *250*, 117181.
(28) Nemiwal, M.; Sillanpaa, M.; Banat, F.; Kumar, D. CeO 2 -Encapsulated Metal Nanoparticles : Synthesis, Properties and Catalytic Applications. *Inorganic Chemistry Communications* **2022**, *143*, 109739.
(29) Fauzi, A. A.; Jalil, A. A.; Hassan, N. S.; Aziz, F. F. A.; Azami, M. S.; Hussain, I.; Saravanan, R.; Vo, D. V. N. A Critical Review on Relationship of CeO2-Based Photocatalyst towards Mechanistic Degradation of Organic Pollutant. *Chemosphere* **2022**, *286*, 131651.
(30) Wang, J.; Xiao, X.; Liu, Y.; Pan, K.; Pang, H.; Wei, S. The Application of CeO2-Based Materials in Electrocatalysis. *J. Mater. Chem. A* **2019**, *7* (30), 17675−17702.
(31) Hezam, A.; Namratha, K.; Drmosh, Q. A.; Ponnamma, D.; Wang, J.; Prasad, S.; Ahamed, M.; Cheng, C.; Byrappa, K. CeO2 Nanostructures Enriched with Oxygen Vacancies for Photocatalytic CO2 Reduction. *ACS Appl. Nano Mater.* **2020**, *3* (1), 138−148.
(32) Castleton, C. W. M.; Lee, A. L.; Kullgren, J.; Hermansson, K. Description of Polarons in Ceria Using Density Functional Theory. *J. Phys. Conf. Ser.* **2014**, *526*, 012002.
(33) Patsalas, P.; Logothetidis, S.; Sygellou, L.; Kennou, S. Structure-Dependent Electronic Properties of Nanocrystalline Cerium Oxide Films. *Phys. Rev. B - Condens. Matter Mater. Phys.* **2003**, *68* (11), 1−13.
(34) Vangelista, S.; Piagge, R.; Ek, S.; Sarnet, T.; Ghidini, G.; Lamperti, A. Atomic Layer Deposition of Cerium Dioxide Film on TiN and Si Substrates: Structural and Chemical Properties. *MRS Adv.* **2017**, *2* (52), 3005−3010.
(35) James, J.; Unni, A. B.; Taleb, K.; Chapel, J. P.; Kalarikkal, N.; Varghese, S.; Vignaud, G.; Grohens, Y. Surface Engineering of Polystyrene-Cerium Oxide Nanocomposite Thin Films for Refractive Index Enhancement. *Nano-Structures and Nano-Objects* **2019**, *17*, 34−42.
(36) Chiu, F.-C.; Lai, C.-M. Optical and Electrical Characterizations of Cerium Oxide Thin Films. *J. Phys. D. Appl. Phys.* **2010**, *43* (7), 075104.
(37) Rajendran, S.; Khan, M. M.; Gracia, F.; Qin, J.; Gupta, V. K.; Arumainathan, S. Ce3+-Ion-Induced Visible-Light Photocatalytic Degradation and Electrochemical Activity of ZnO/CeO2 Nanocomposite. *Sci. Rep.* **2016**, *6* (April), 1−11.
(38) Matussin, S. N.; Khan, M. M. Phytogenic Fabrication of CeO2@SnO2 Heterojunction Nanostructures for Antioxidant Studies. *Chem. Pap.* **2022**, *76* (4), 2071−2084.
(39) Saravanan, R.; Agarwal, S.; Gupta, V. K.; Khan, M. M.; Gracia, F.; Mosquera, E.; Narayanan, V.; Stephen, A. Line Defect Ce3+ Induced Ag/CeO2/ZnO Nanostructure for Visible-Light Photocatalytic Activity. *J. Photochem. Photobiol. A Chem.* **2018**, *353*, 499−506.
(40) Khan, M. M.; Ansari, S. A.; Pradhan, D.; Han, D. H.; Lee, J.; Cho, M. H. Defect-Induced Band Gap Narrowed CeO2 Nanostructures for Visible Light Activities. *Ind. Eng. Chem. Res.* **2014**, *53* (23), 9754−9763.
(41) Ansari, S. A.; Khan, M. M.; Ansari, M. O.; Kalathil, S.; Lee, J.; Cho, M. H. Band Gap Engineering of CeO2 Nanostructure Using an Electrochemically Active Biofilm for Visible Light Applications. *RSC Adv.* **2014**, *4* (32), 16782−16791.
(42) Khan, M. M.; Ansari, S. A.; Ansari, M. O.; Min, B. K.; Lee, J.; Cho, M. H. Biogenic Fabrication of Au@CeO2 Nanocomposite with Enhanced Visible Light Activity. *J. Phys. Chem. C* **2014**, *118* (18), 9477−9484.
(43) Khan, M. M.; Ansari, S. A.; Lee, J. H.; Ansari, M. O.; Lee, J.; Cho, M. H. Electrochemically Active Biofilm Assisted Synthesis of Ag@CeO2 Nanocomposites for Antimicrobial Activity, Photocatalysis and Photoelectrodes. *J. Colloid Interface Sci.* **2014**, *431*, 255−263.
(44) Schmitt, R.; Nenning, A.; Kraynis, O.; Korobko, R.; Frenkel, A. I.; Lubomirsky, I.; Haile, S. M.; Rupp, J. L. M. A Review of Defect Structure and Chemistry in Ceria and Its Solid Solutions. *Chem. Soc. Rev.* **2020**, *49* (2), 554−592.
(45) Sisubalan, N.; Karthikeyan, C.; Senthil Kumar, V.; Varaprasad, K.; Haja Hameed, A. S. a.; Vanajothi, R.; Sadiku, R. Biocidal Activity of Ba^{2+}-Doped CeO_2 NPs against *Streptococcus mutans* and *Staphylococcus aureus* Bacterial Strains. *RSC Adv.* **2021**, *11* (49), 30623−30634.
(46) Singh, K. R. B.; Nayak, V.; Sarkar, T.; Singh, R. P. Cerium Oxide Nanoparticles: Properties, Biosynthesis and Biomedical Application. *RSC Adv.* **2020**, *10* (45), 27194−27214.
(47) Scirè, S.; Palmisano, L. *Cerium and Cerium Oxide: A Brief Introduction*; Elsevier Inc., 2020; p 1, DOI: 10.1016/B978-0-12-815661-2.00001-3.
(48) Qadeer, N.; Jabeen, N.; Khan, L. U.; Sohail, M.; Zaheer, M.; Vaqas, M.; Kanwal, A.; Sajid, F.; Qamar, S.; Akhter, Z. Hydrothermal Synthesis and Characterization of Transition Metal (Mn/Fe/Cu) Co-Doped Cerium Oxide-Based Nano-Additives for Potential Use in the Reduction of Exhaust Emission from Spark Ignition Engines. *RSC Adv.* **2022**, *12* (24), 15564−15574.
(49) Miri, A.; Sarani, M.; Khatami, M. Nickel-Doped Cerium Oxide Nanoparticles: Biosynthesis, Cytotoxicity and UV Protection Studies. *RSC Adv.* **2020**, *10* (7), 3967−3977.
(50) Derafa, W.; Paloukis, F.; Mewafy, B.; Baaziz, W.; Ersen, O.; Petit, C.; Corbel, G.; Zafeiratos, S. Synthesis and Characterization of Nickel-Doped Ceria Nanoparticles with Improved Surface Reducibility. *RSC Adv.* **2018**, *8* (71), 40712−40719.
(51) Naidi, S. N.; Khan, F.; Harunsani, M. H.; Tan, A. L.; Kim, Y. M.; Khan, M. M. Effect of Zr Doping on Photoantioxidant and Antibiofilm Properties of CeO2 NPs Fabricated Using Aqueous Leaf Extract of Pometia Pinnata. *Bioprocess Biosyst. Eng.* **2022**, *45* (2), 279−295.
(52) Lu, B.; Zhang, T.; Zhang, L.; Xu, Y.; Zhang, Z.; Wu, F.; Li, X.; Luo, C. Promotion Effects of Oxygen Vacancies on Activity of Na-Doped CeO2 Catalysts for Reverse Water Gas Shift Reaction. *Appl. Surf. Sci.* **2022**, *587*, 152881.
(53) Ang, M. L.; Oemar, U.; Saw, E. T.; Mo, L.; Kathiraser, Y.; Chia, B. H.; Kawi, S. Highly Active Ni/XNa/CeO2catalyst for the Water-Gas Shift Reaction: Effect of Sodium on Methane Suppression. *ACS Catal.* **2014**, *4* (9), 3237−3248.
(54) Gnanamani, M. K.; Jacobs, G.; Martinelli, M.; Shafer, W. D.; Hopps, S. D.; Thomas, G. A.; Davis, B. H. Dehydration of 1,5-Pentanediol over Na-Doped CeO2 Catalysts. *ChemCatChem* **2018**, *10* (5), 1148−1154.
(55) Gnanamani, M. K.; Jacobs, G.; Shafer, W. D.; Davis, B. H. Dehydration of 2-Octanol over Ca-Doped CeO2 Catalysts. *ChemCatChem* **2017**, *9* (3), 492−498.
(56) Ramasamy, V.; Mohana, V.; Rajendran, V. Characterization of Ca Doped CeO2 Quantum Dots and Their Applications in Photocatalytic Degradation. *OpenNano* **2018**, *3*, 38−47.
(57) Murugan, R.; Kashinath, L.; Subash, R.; Sakthivel, P.; Byrappa, K.; Rajendran, S.; Ravi, G. Pure and Alkaline Metal Ion (Mg, Ca, Sr, Ba) Doped Cerium Oxide Nanostructures for Photo Degradation of Methylene Blue. *Mater. Res. Bull.* **2018**, *97*, 319−325.
(58) Li, L.; Tan, R.; Luo, S.; Jiang, C.; Jing, F. Controlled Reaction Depth by Metal (M = Fe, Ni, Mn and Ti) Doped Ceria in Selective Oxidation of Ethane with Carbon Dioxide. *Appl. Catal. A Gen.* **2022**, *635*, 118565.
(59) Hołówko, B.; Błaszczak, P.; Chlipała, M.; Gazda, M.; Wang, S. F.; Jasiński, P.; Bochentyn, B. Structural and Catalytic Properties of Ceria Layers Doped with Transition Metals for SOFCs Fueled by Biogas. *Int. J. Hydrogen Energy* **2020**, *45* (23), 12982−12996.
(60) Kurajica, S.; Mužina, K.; Dražić, G.; Matijašić, G.; Duplančić, M.; Mandić, V.; Župančić, M.; Munda, I. K. A Comparative Study of Hydrothermally Derived Mn, Fe, Co, Ni, Cu and Zn Doped Ceria Nanocatalysts. *Mater. Chem. Phys.* **2020**, *244*, 122689.
(61) Myung, J. H.; Shin, T. H.; Huang, X.; Carins, G.; Irvine, J. T. S. Enhancement of Redox Stability and Electrical Conductivity by Doping Various Metals on Ceria, Ce1-XMxO2-δ (M = Ni, Cu, Co, Mn, Ti, Zr). *Int. J. Hydrogen Energy* **2015**, *40* (35), 12003−12008.
(62) Tabakova, T.; Ilieva, L.; Ivanov, I.; Zanella, R.; Sobczak, J. W.; Lisowski, W.; Kaszkur, Z.; Andreeva, D. Influence of the Preparation

https://doi.org/10.1021/acsomega.3c01199
ACS Omega XXXX, XXX, XXX−XXX

Method and Dopants Nature on the WGS Activity of Gold Catalysts Supported on Doped by Transition Metals Ceria. *Appl. Catal. B Environ.* **2013**, *136−137*, 70−80.
(63) Venkataswamy, P.; Jampaiah, D.; Kandjani, A. E.; Sabri, Y. M.; Reddy, B. M.; Vithal, M. Transition (Mn, Fe) and Rare Earth (La, Pr) Metal Doped Ceria Solid Solutions for High Performance Photocatalysis: Effect of Metal Doping on Catalytic Activity. *Res. Chem. Intermed.* **2018**, *44* (4), 2523−2543.
(64) Li, S.; Wang, N.; Yue, Y.; Wang, G.; Zu, Z.; Zhang, Y. Copper Doped Ceria Porous Nanostructures towards a Highly Efficient Bifunctional Catalyst for Carbon Monoxide and Nitric Oxide Elimination. *Chem. Sci.* **2015**, *6* (4), 2495−2500.
(65) Ansari, A. A.; Labis, J. P.; Alam, M.; Ramay, S. M.; Ahmad, N.; Mahmood, A. Synthesis, Structural and Optical Properties of Mn-Doped Ceria Nanoparticles: A Promising Catalytic Material. *Acta Metall. Sin. (English Lett.* **2016**, *29* (3), 265−273.
(66) Kumar, P.; Kumar, P.; Kumar, A.; Meena, R. C.; Tomar, R.; Chand, F.; Asokan, K. Structural, Morphological, Electrical and Dielectric Properties of Mn Doped CeO2. *J. Alloys Compd.* **2016**, *672*, 543−548.
(67) Beena, S.; Abraham, N.; Suresh Babu, V. Facile Synthesis and Characterization Studies of Mn Co-Doped Ceria Nanoparticles: A Promising Electrode Material for Supercapacitors. *Mater. Today Proc.* **2023**, *80*, 2280.
(68) K.C, R.; N.N, B. Cobalt Doped Ceria Catalysts for the Oxidative Abatement of Gaseous Pollutants and Colorimetric Detection of H2O2. *Mater. Res. Bull.* **2021**, *139*, 111253.
(69) Jiang, S.; Zhang, R.; Liu, H.; Rao, Y.; Yu, Y.; Chen, S.; Yue, Q.; Zhang, Y.; Kang, Y. Promoting Formation of Oxygen Vacancies in Two-Dimensional Cobalt-Doped Ceria Nanosheets for Efficient Hydrogen Evolution. *J. Am. Chem. Soc.* **2020**, *142* (14), 6461−6466.
(70) Matussin, S. N.; Khan, F.; Harunsani, M. H.; Kim, Y.-M.; Khan, M. M. Visible-Light-Induced Photocatalytic and Photoantibacterial Activities of the Co-Doped CeO2. *ACS Omega* **2023**, *8*, 11868.
(71) Lee, C. E.; Choi, S. H.; Kim, H. Y.; Lee, S. S.; Kim, S. K.; An, K.-S. Enhanced Pseudocapacitive Performances of Eco-Friendly Co-Precipitated Fe-Doped Cerium Oxide Nanoparticles. *Ceram. Int.* **2021**, *47* (15), 21988−21995.
(72) Rahdar, A.; Aliahmad, M.; Samani, M.; HeidariMajd, M.; Susan, M. A. B. H. Synthesis and Characterization of Highly Efficacious Fe-Doped Ceria Nanoparticles for Cytotoxic and Antifungal Activity. *Ceram. Int.* **2019**, *45* (6), 7950−7955.
(73) Adegoke, O.; Daeid, N. N. Polymeric-Coated Fe-Doped Ceria/Gold Hybrid Nanocomposite as an Aptasensor for the Catalytic Enhanced Colorimetric Detection of 2,4-Dinitrophenol. *Colloids Surfaces A Physicochem. Eng. Asp.* **2021**, *627* (July), 127194.
(74) Venkataswamy, P.; Damma, D.; Jampaiah, D.; Mukherjee, D.; Vithal, M.; Reddy, B. M. Cr-Doped CeO2 Nanorods for CO Oxidation: Insights into Promotional Effect of Cr on Structure and Catalytic Performance. *Catal. Lett.* **2020**, *150* (4), 948−962.
(75) Riaz, A.; Kremer, F.; Kim, T.; Sattayaporn, S.; Tsuzuki, T.; Lipiński, W.; Lowe, A. Experimental Demonstration of Vanadium-Doped Nanostructured Ceria for Enhanced Solar Thermochemical Syngas Production. *Nano Energy* **2021**, *81*, 105639.
(76) Aseena, S.; Abraham, N.; Suresh Babu, V. Morphological and Optical Studies of Zinc Doped Cerium Oxide Nanoparticles Prepared by Single Step Co-Precipitation Method. *Mater. Today Proc.* **2023**, *80*, 1901.
(77) Ramasamy, V.; Vijayalakshmi, G. Synthesis, Characterization and Tuning of Visible Region Absorption Ability of Cadmium Doped Ceria Quantum Dots. *J. Mater. Sci. Mater. Electron.* **2016**, *27* (5), 4723−4735.
(78) Maleki, P.; Nemati, F.; Gholoobi, A.; Hashemzadeh, A.; Sabouri, Z.; Darroudi, M. Green Facile Synthesis of Silver-Doped Cerium Oxide Nanoparticles and Investigation of Their Cytotoxicity and Antibacterial Activity. *Inorg. Chem. Commun.* **2021**, *131* (June), 108762.
(79) Ameur, N.; Fandi, Z.; Taieb-Brahimi, F.; Ferouani, G.; Bedrane, S.; Bachir, R. A Novel Approach of Ceria Nanotubes and Plasmonic Metal-Doped Ceria Nanotubes Application: Anticorrosion and Photodegradation Potential. *Appl. Phys. A Mater. Sci. Process.* **2021**, *127* (3), 1−12.
(80) Liu, H.; Zhu, Y.; Ma, J.; Chen, C.; Cheng, P.; Zhang, S. Hydrothermal Synthesis of Pd-Doped CeO2 Nanomaterials and Electrochemical Detection for Phenol. *J. Cryst. Growth* **2022**, *586* (March), 126626.
(81) Saravanakumar, K.; Sathiyaseelan, A.; Priya, V. V.; Wang, M. H. PEGylated Palladium Doped Ceria Oxide Nanoparticles (Pd-Dop-CeO2-PEG NPs) for Inhibition of Bacterial Pathogens and Human Lung Cancer Cell Proliferation. *J. Drug Delivery Sci. Technol.* **2022**, *72* (April), 103367.
(82) Matussin, S. N.; Khan, F.; Harunsani, M. H.; Kim, Y. M.; Khan, M. M. Effect of Pd-Doping Concentrations on the Photocatalytic, Photoelectrochemical, and Photoantibacterial Properties of CeO2. *Catalysts* **2023**, *13* (1), 96.
(83) Manibalan, G.; Murugadoss, G.; Hazra, S.; Marimuthu, R.; Manikandan, C.; Jothi Ramalingam, R.; Rajesh Kumar, M. A Facile Synthesis of Sn-Doped CeO2 Nanoparticles: High Performance Electrochemical Nitrite Sensing Application. *Inorg. Chem. Commun.* **2022**, *135*, 109096.
(84) Santra, C.; Auroux, A.; Chowdhury, B. Bi Doped CeO2 Oxide Supported Gold Nanoparticle Catalysts for the Aerobic Oxidation of Alcohols. *RSC Adv.* **2016**, *6* (51), 45330−45342.
(85) Shehata, N.; Meehan, K.; Ashry, I.; Kandas, I.; Xu, Y. Lanthanide-Doped Ceria Nanoparticles as Fluorescence-Quenching Probes for Dissolved Oxygen. *Sensors Actuators, B Chem.* **2013**, *183*, 179−186.
(86) Kannan, K.; Radhika, D.; Nesaraj, A. S.; Revathi, V.; Sadasivuni, K. K. A Simple Chemical Precipitation of Ceria Based (Sm Doped-CGO) Nanocomposite: Structural and Electrolytic Behaviour for LT-SOFCs. *SN Appl. Sci.* **2020**, *2* (7), 1−9.
(87) Deng, T.; Zhang, C.; Xiao, Y.; Xie, A.; Pang, Y.; Yang, Y. One-Step Synthesis of Samarium-Doped Ceria and Its CO Catalysis. *Bull. Mater. Sci.* **2015**, *38* (5), 1149−1154.
(88) Bregman, A.; Rimsza, J.; Ringgold, M.; Bell, N.; Treadwell, L. R. The Role of Precursor Decomposition in the Formation of Samarium Doped Ceria Nanoparticles via Solid-State Microwave Synthesis. *SN Appl. Sci.* **2021**, *3* (3), 1−11.
(89) Wattanathana, W.; Veranitisagul, C.; Wannapaiboon, S.; Klysubun, W.; Koonsaeng, N.; Laobuthee, A. Samarium Doped Ceria (SDC) Synthesized by a Metal Triethanolamine Complex Decomposition Method: Characterization and an Ionic Conductivity Study. *Ceram. Int.* **2017**, *43* (13), 9823−9830.
(90) Anantharaman, A. P.; Gadiyar, H. J.; Surendran, M.; Rao, A. S.; Dasari, H. P.; Dasari, H.; Babu, G. U. B. Effect of Synthesis Method on Structural Properties and Soot Oxidation Activity of Gadolinium-Doped Ceria. *Chem. Pap.* **2018**, *72* (12), 3179−3188.
(91) Popov, A. L.; Abakumov, M. A.; Savintseva, I. V.; Ermakov, A. M.; Popova, N. R.; Ivanova, O. S.; Kolmanovich, D. D.; Baranchikov, A. E.; Ivanov, V. K. Biocompatible Dextran-Coated Gadolinium-Doped Cerium Oxide Nanoparticles as MRI Contrast Agents with High: T 1relaxivity and Selective Cytotoxicity to Cancer Cells. *J. Mater. Chem. B* **2021**, *9* (33), 6586−6599.
(92) Shi, G.; Tano, T.; Tryk, D. A.; Iiyama, A.; Uchida, M.; Kuwauchi, Y.; Masuda, A.; Kakinuma, K. Pt Nanorods Oriented on Gd-Doped Ceria Polyhedra Enable Superior Oxygen Reduction Catalysis for Fuel Cells. *J. Catal.* **2022**, *407*, 300−311.
(93) Ortega, P. P.; Hangai, B.; Moreno, H.; Rocha, L. S. R.; Ramírez, M. A.; Ponce, M. A.; Longo, E.; Simões, A. Z. Tuning Structural, Optical, and Gas Sensing Properties of Ceria-Based Materials by Rare-Earth Doping. *J. Alloys Compd.* **2021**, *888*, 161517.
(94) Lin, L.; Ma, X.; Li, S.; Wouters, M.; Hessel, V. Plasma-Electrochemical Synthesis of Europium Doped Cerium Oxide Nanoparticles. *Front. Chem. Sci. Eng.* **2019**, *13* (3), 501−510.
(95) Sahoo, S. K.; Mohapatra, M.; Anand, S. Characterization and Optical Properties of Eu-Doped Cubic Nano Ceria Synthesized by Using the Co-Precipitation-Hydrothermal Route. *J. Korean Phys. Soc.* **2013**, *62* (2), 297−304.

https://doi.org/10.1021/acsomega.3c01199
ACS Omega XXXX, XXX, XXX−XXX

(96) Li, Q.; Sun, M.; Su, Y.; Zhang, K.; Lv, Y. Efficient Chemiluminescence Resonance Energy Transfer on the Interface of Europium Doped Ceria for Sulfite Detection in PM2.5. *Sensors Actuators, B Chem.* **2021**, *339*, 129876.
(97) Xiao, Z.; Ji, S.; Li, Y.; Hou, F.; Zhang, H.; Zhang, X.; Wang, L.; Li, G. Tuning Oxygen Vacancies on Mesoporous Ceria Nanorods by Metal Doping: Controllable Magnetic Property. *Appl. Surf. Sci.* **2018**, *455* (June), 1037−1044.
(98) Chahal, S.; Singh, S.; Kumar, A.; Kumar, P. Oxygen-Deficient Lanthanum Doped Cerium Oxide Nanoparticles for Potential Applications in Spintronics and Photocatalysis. *Vacuum* **2020**, *177* (April), 109395.
(99) Oliveira, L. L.; Cortés, J. A.; Caldeira, B. S.; Strusch, T.; Wiedwald, U.; Simoes, A. Z. Structural, Electronic Paramagnetic Resonance and Magnetic Properties of Praseodymium-Doped Rare Earth CeO2 Semiconductors. *Ceram. Int.* **2021**, *47*, 20768−20780.
(100) Sandhya, K.; Chitra Priya, N. S.; Rajendran, D. N.; Thappily, P. Structural and Electrical Properties of Cerium Oxides Doped by Sb3+ and Bi3+ Cations. *J. Electron. Mater.* **2020**, *49* (8), 4936−4944.
(101) Kabir, A.; Bowen, J. R.; Varenik, M.; Lubomirsky, I.; Esposito, V. Enhanced Electromechanical Response in Sm and Nd Co-Doped Ceria. *Materialia* **2020**, *12*, 100728.
(102) Zhan, S.; Huang, H.; He, C.; Xiong, Y.; Li, P.; Tian, S. Controllable Synthesis of Substitutional and Interstitial Nitrogen-Doped Ceria: The Effects of Doping Sites on Enhanced Catalytic Ozonation of Organic Pollutants. *Appl. Catal. B Environ.* **2023**, *321*, 122040.
(103) Mansingh, S.; Padhi, D. K.; Parida, K. M. Enhanced Visible Light Harnessing and Oxygen Vacancy Promoted N, S Co-Doped CeO2 Nanoparticle: A Challenging Photocatalyst for Cr(vi) Reduction. *Catal. Sci. Technol.* **2017**, *7* (13), 2772−2781.
(104) Yang, H.; Jia, L.; Haraguchi, J.; Wang, Y.; Xu, B.; Zhang, Q.; Nan, Z.; Zhang, M.; Ohno, T. Nitrogen and Sulfur Co-Doped CeO2 Nanorods for Efficient Photocatalytic VOCs Degradation. *Catal. Sci. Technol.* **2022**, *12* (16), 5203−5209.
(105) Han, Z.; Li, Z.; Li, Y.; Shang, D.; Xie, L.; Lv, Y.; Zhan, S.; Hu, W. Enhanced Electron Transfer and Hydrogen Peroxide Activation Capacity with N, P-Codoped Carbon Encapsulated CeO2 in Heterogeneous Electro-Fenton Process. *Chemosphere* **2022**, *287*, 132154.
(106) Gong, K.; Zhou, K.; Yu, B. Superior Thermal and Fire Safety Performances of Epoxy-Based Composites with Phosphorus-Doped Cerium Oxide Nanosheets. *Appl. Surf. Sci.* **2020**, *504*, 144314.
(107) Basha, M. H.; Gopal, N. O. Solution Combustion Synthesis and Characterization of Phosphorus Doped TiO2-CeO2 Nanocomposite for Photocatalytic Applications. *Mater. Sci. Eng. B Solid-State Mater. Adv. Technol.* **2018**, *236*−*237*, 43−47.
(108) Tao, X.; Yang, Z.; Cheng, M.; Yan, R.; Chen, F.; Cao, S.; Li, S.; Ma, T.; Cheng, C.; Yang, W. Phosphorus Modulated Porous CeO2 Nanocrystallines for Accelerated Polysulfide Catalysis in Advanced Li-S Batteries. *J. Mater. Sci. Technol.* **2022**, *131*, 212−220.
(109) Yang, B.; Zhang, M.; Zeng, Y.; Meng, F.; Ma, J.; Zhang, S.; Zhong, Q. Promotional Effect of Surface Fluorine Species on CeO2 Catalyst for Toluene Oxidation. *Mol. Catal.* **2021**, *512*, 111771.
(110) Fan, X.; Feng, Z.; Zeng, M.; Zhou, T.; Zuo, Y.; Liang, Z.; Zhan, L.; Zhou, X.; Zhang, Y. Tuning the Surface Structure of CeO2 Nanoparticles by Chlorine-Doped Strategy to Improve the Polysulfide Reaction Kinetic for Lithium Sulfur Battery. *Colloids Surfaces A Physicochem. Eng. Asp.* **2023**, *659*, 130571.
(111) Chen, J.; Feng, W.; Zhao, W. Anion-Doped CeO2 for High-Performance Lithium-Sulfur Batteries. *Appl. Surf. Sci.* **2022**, *584*, 152613.
(112) Shao-You, L.; Cheng-Gang, Z.; Shi-Biao, Z.; Wei-Guo, Z.; Qing-Ge, F. Sulfur Doped Ceria Mesoporous Nanomaterial: Solid-State Synthesis, Characterization and Photocatalytic Property of Methyl Orange. *Sci. Adv. Mater.* **2018**, *10* (2), 155−164.
(113) Matussin, S. N.; Harunsani, M. H.; Khan, M. M. CeO2 and CeO2-Based Nanomaterials for Photocatalytic, Antioxidant and Antimicrobial Activities. *J. Rare Earths* **2023**, *41* (2), 167−181.

https://doi.org/10.1021/acsomega.3c01199
ACS Omega XXXX, XXX, XXX−XXX